



Research Article

Material Composition of Greenstone Acquisition and Use in the Jovel Valley, Chiapas, Mexico

Jennifer L. Meanwell¹ , Elizabeth H. Paris²  and Roberto López Bravo³ 

¹Center for Materials Research in Archaeology and Ethnology, Massachusetts Institute of Technology, 77 Massachusetts Ave., Cambridge, MA, 02139, USA; ²Department of Anthropology and Archaeology, University of Calgary, 2500 University Drive NW, ES 620, Calgary, AB, T2N 1N4, Canada and ³Licenciatura en Arqueología, Facultad de Humanidades, Universidad de Ciencias y Artes de Chiapas, Antiguo Camino a San Gabriel s/n, C.P. 29160, Chiapa de Corzo, Chiapas, Mexico.

Abstract

Greenstone is commonly used to produce culturally significant items across Mesoamerica, including axes, earspools, figurines, and beads. This research characterizes the mineralogy of greenstone materials recovered from sites in the Jovel Valley, Chiapas, Mexico, to document the range of green minerals utilized by the inhabitants. Our analysis of the objects suggests that the Late Classic and Early Postclassic Maya of the Jovel Valley had access to a variety of greenstone minerals, including serpentinites, green micas, grossular, and jadeite. X-ray diffraction and X-ray fluorescence spectrometry characterization of reference materials suggests procurement of greenstone resources from the well-documented sources of the Motagua–Polochnic Fault Zone, and also potentially from sources in the Chalchihuitán–Chenalhó area of Chiapas, Mexico. The Jovel Valley had access to materials over long distances through historically documented trade routes that allowed the movement of greenstone materials west from the Motagua River Valley into highland Chiapas or south from the Chalchihuitán–Chenalhó area.

For the ancient Maya, green represented the color of life; the color of ripe vegetation; the color of water in rivers and lakes; the color of unripe corn; the color of the resplendent quetzal; the color whose very name “yax” meant “precious” (Houston et al. 2009; Pendergast 1998). From the Early Formative period and beyond, we see archaeological evidence for the use of greenstone as a precious material at Maya sites (Hammond et al. 1977:41), and also more broadly throughout the early Mesoamerican world (Diehl 2005; Garber et al. 1993; Ortiz and Rodríguez 2000). Greenstone was used to produce culturally significant items such as beads, figurines, earspools, and other personal adornments, although in rare instances it was also used to create sculptures and monuments, such as the serpentine pavements of Middle Formative period La Venta (Clark and Coleman 2014; Drucker et al. 1959), or the carved jade sculpture of Sun God’s head at Classic period Altun Ha (Pendergast 1982). These items were often used for wealth accumulation, adornment, status symbols, and precious offerings in caches and funerary contexts (Kovacevich and Callaghan 2019).

Many green minerals and rocks were used in Mesoamerica to make objects and ornaments; for this reason, many Mesoamericanists use the terms “greenstone” or “social jade” rather than “jade” (Powis et al. 2016; Tremain 2014). The majority of jade deposits are highly heterogeneous and are frequently associated with other minerals, many of which are also green in color (Bishop et al. 1985; Bishop et al. 1993a, Bishop et al. 1993b). Many scholars have noted cultural preferences for certain colors and characteristics concerning the social value of different greenstones, including Olmec preferences for blue-green hues and Late Classic period Maya rulers’ preferences for apple-green colors (Seitz et al. 2001; Taube et al. 2004). Pendergast (1998:4) argues that some utilitarian items, such as woodworking axes, favored dark greenish-black materials.

In this paper, we present the analysis of greenstone artifacts recovered from Late Classic to Early Postclassic sites in the Jovel Valley, Chiapas, Mexico. These objects were excavated during the “Proyecto Económico de los Altos de Chiapas” and “Proyecto Interacción Entre Reinos en los Altos de Chiapas,” both directed by Dr. Elizabeth Paris and Dr. Roberto López Bravo, and were exported to MIT with permission from the Consejo de Arqueología del INAH, Mexico. We present new mineralogical and compositional analysis of these artifacts using X-ray diffraction (XRD) and X-ray fluorescence spectrometry (XRF), and our

Corresponding author: Elizabeth H. Paris; Email: elizabeth.paris@ucalgary.ca

Cite this article: Meanwell, Jennifer L., Elizabeth H. Paris, and Roberto López Bravo (2025) Material Composition of Greenstone Acquisition and Use in the Jovel Valley, Chiapas, Mexico. *Ancient Mesoamerica* 1–25. <https://doi.org/10.1017/S095653612500001X>

findings indicate that Jovel Valley residents were utilizing a wide variety of greenstones, including both jadeites and “social jades” in both everyday and ritual practice. We also characterize the mineralogy of comparative greenstone samples from sources in highland Guatemala and highland Chiapas attributed to the Chalchihuitán area to evaluate the range of greenstone materials available at Jovel Valley sites, and hopefully provide comparative data for further investigations. Our results indicate that Jovel Valley residents used a wide variety of valuable green minerals in addition to jadeites, including micaceous stones, quartz, albite, and serpentinite.

Background

Known greenstone deposits in Mesoamerica

Mineralogists recognize two minerals, one amphibole and one pyroxene, as true “jade.” The amphibole jade, called nephrite, is not present in Mesoamerican geological deposits, and has not been identified to date in any of the known Mesoamerican sources (Hammond et al. 1977:41). Jadeite is a pyroxene group mineral, and is often found in solid solution with other pyroxene group minerals. Pyroxene-based jades are traditionally classified according to the relative proportions of their three principal components: jadeite ($\text{NaAlSi}_2\text{O}_6$), diopside ($\text{CaMgSi}_2\text{O}_6$) and aegirine ($\text{NaFe}^{+3}\text{Si}_2\text{O}_6$). Rocks that consist almost entirely of jadeite are called jadeite

(with less than 20 percent diopside+aegirine), while a solid solution of jadeite and diopside with less than 20 percent aegirine is called “omphacite jade.” Chloromelanite is a type of iron-rich jade with more than 20 percent aegirine (Hammond et al. 1977:41), and often ranges in color from dark green to black (Foshag 1957:23). More recently, Franz and others (2014) have proposed a new system of classification for jades, with the three principal minerals jadeite, diopside, and kosmochlor ($\text{NaCrSi}_2\text{O}_6$). Complicating geological sourcing, jadeite is commonly found near associated minerals that can also have a green color, such as serpentinite, kosmochlor, and clinoamphiboles.

The best-known deposits of jadeite in Mesoamerica are located in the Motagua River Valley in Guatemala (Figure 1); these are thought to have provided most of the jadeite artifacts from Mesoamerican sites, although specific source locations are often a closely guarded secret (Hammond et al. 1977). The Motagua–Polochic Fault System extends over 200 km along the Motagua River from its tributaries in the western Guatemalan highlands, east to Lake Izabal, with a range of jadeite and serpentinite-bearing locations to both north and south of the river (Gendron et al. 2002; Harlow et al. 2011; Mora et al. 2007; Smith 2005). Many of the explored jadeite deposits are concentrated on the north bank in the region surrounding San Agustín Acasaguastlán and San Cristóbal Acasaguastlán (Becquelin and Bosc 1973; Bosc 1971; Harlow et al. 1993; Taube et al.



Figure 1. Map of Mesoamerica with sites and greenstone-bearing areas described in the text. Sites emphasized in the text are highlighted in red. Drafted by Elizabeth Paris, from base map by Wikimedia Commons (Sémhur / Wikimedia Commons / CC-BY-4.0), with reference to Powis et al. 2016:Figure 2.

2004), along the western edge of the Sierra de las Minas range. On the south bank, explorations have been concentrated in the Río El Tambor district between Carrizal Grande and La Ensenada (Gendron et al. 2002; Harlow et al. 1993; Harlow et al. 2011). Realistically, jadeite and other associated raw materials likely came from several different sources in the Upper and Middle Motagua regions of Guatemala (Harlow et al. 2011; Hruby 2015; Rochette 2009; Taube and Ishihara-Brito 2012:138–140). Within the Motagua–Polochic Fault System jadeite occurs in small areas, typically extending no more than a few hundred meters, commonly distributed as boulders and cobbles of a dismembered larger body sitting on (and in) serpentinite, where they are identified and mined from near-surface deposits (Harlow et al. 2011:366).

The metamorphic deposits of the Motagua–Polochic Fault System are geologically diverse, where jadeite formed in association with other green minerals. Muscovite ($(K_2Al_4[Si_6Al_2O_{20}](OH, F)_4)$) is a potassium-rich mica, and can be pale green with a flaky, foliated habit; paragonite ($(NaAl_2(AlSi_3O_{10})(OH)_2)$) has a similar structure, with sodium in place of potassium (see also Harlow et al. 2011:369). Paragonite is characteristic of metamorphic zones with schists and eclogites, which is a geology similar to zones where jadeite tends to form. Ephesite ($(NaLiAl_2(Si_2Al_2)O_{10}(OH)_2)$) is a rare mica that is typically associated with chlorite, muscovite, and corundum (Smith 1851). Other green minerals include chlorite ($(Mg, Al, Fe)_{12}[(SiAl)_8O_{20}](OH)_{16}$); soapstone ($(Mg_6[Si_8O_{20}](OH)_4)$); serpentine ($(Mg_6[Si_4O_{10}](OH)_8)$) and other minerals in the serpentine subgroup; albite ($(NaAlSi_3O_8)$); green chalcedony ((SiO_2)); and green marble (metamorphosed limestone ($(CaCO_3)$) or dolomite ($(CaMg(CO_3)_2)$) (Hammond et al. 1977:41). Another mineral that may be green is olivine, a ferric silicate rich in magnesium ($(Mg^{2+}, Fe^{2+})_2SiO_4$) that weathers rapidly at the surface, and the broader olivine group that includes tephroite ((Mn_2SiO_4)), monticellite ($(CaMgSiO_4)$) and kirschsteinite ($(CaFeSiO_4)$). The Motagua–Polochic Fault System deposits also contains grossular ($(Ca_3Al_2[SiO_4]_3)$), a rare, green variety of garnet, which occurs both north of the fault, and also south of it in the region around La Ensenada (Harlow et al. 2011:376).

Harlow and others (2011:365) argue that there are some significant differences between the geologies of the north and south sides of the Motagua–Polochic Fault. To the north the serpentinite deposits contain a variety of minerals including garnet amphibolite, omphacite-taramite metabasite, jadeitite, albitite, and altered clinzoisite-amphibole-eclogite on the western edge; while to the south, assemblages feature lawsonite, eclogite, blueschist, and jadeitite (see also Becquelin and Bosc 1973; Gendron et al. 2002; Smith 2005). Greenstone in the deposits north of the Motagua Fault predominantly features paragonite mica, while deposits to the south lack paragonite and contain abundant muscovite deposits (Harlow et al. 2011:384). Finally, Harlow and others (2011:380–381) argue that none of the jadeitites to the north of the Motagua Fault contain quartz, either as inclusions in jadeite or in veins, but all contain albite, mica, and usually analcime; jadeites from south

of the Motagua Fault, in contrast, frequently present quartz inclusions in jadeitite.

Several other regions in Mesoamerica bear slightly different ranges of metamorphic geological materials that appear green, many of which were exploited in pre-Columbian times; however, they are not known to contain jadeite (Figure 1). The Acatlán Complex extends across areas centered principally within the modern state of Guerrero. As observed also in the Motagua–Polochic Fault System, many of these deposits include grossular ($(Ca_3Al_2[SiO_4]_3)$), which is also relatively common in northern Mexico. Powis and others (2016:69) suggest that some of the basalts and kyanite-bearing metamorphic triangulate stones found at Middle Preclassic sites in Belize can be attributed to the Acatlán Complex. Serpentinite (antigorite) deposits have been identified at the Tehuizingo quarry in southern Puebla, and Cuicatlan quarry in northwest Oaxaca, supplying some of the celts recovered from the Olmec sites of La Merced and La Venta (Jaime-Riverón et al. 2009). Smith and Gendron (1997) also document the use of eclogite in greenstone axes at Cozumel Island, eclogite being a rare, dense high-P metamorphic rock composed largely of red [pyrope + almandine]-rich garnet and green [jadeite + diopside]-rich clinopyroxene, but in which other minerals may be extremely variable in quantity and in chemical composition; they note that eclogite minerals are present in both the Motagua–Polochic Fault System and the Acatlán Complex. The Maya Mountains of central Belize (Bladen Formation) also contain kyanite-bearing schists and other medium- to high-grade metamorphic rocks including dark-green metamorphosed basalts comprised principally of chlorite ((ClO_2^-) ; Powis et al. 2016:63).

Other minerals that exhibit green or blue coloring, which can be detected due to the presence of copper, include malachite ($(Cu_2(CO_3)(OH)_2)$), azurite ($(Cu_3(CO_3)_2(OH)_2)$), veszelyite ($(Cu, Zn) 2ZnPO_4(OH)_3 \cdot 2(H_2O)$) and turquoise ($(CuAl_6(PO_4)_4(OH)_8 \cdot 4H_2O)$). While the principal sources of copper ores are located in West and Central Mexico (Hosler 1994), small pockets of malachite, azurite, and chalcocopyrite are located at several locations in the Maya area, including the western Teapa Valley (Santa Fe mine area) of southern Tabasco (Manrique-Ortega et al. 2020b), Las Chicharras (Pacific Coastal Chiapas; González Cruz 2011:206) as well as some locations in Guatemala in a west–east band along the northern edge of the Cuchumatanes and Sierra Madre mountain ranges (Weeks 2013:121). To date, the only Maya site with published evidence for pre-Hispanic copper ore processing and smelting is that of El Coyote in Honduras (Urban et al. 2013), with evidence of copper remelting and casting at Late Postclassic cities such as K'umarkaj (Utatlán; Weeks 2013), Mayapan (Meanwell et al. 2013; Meanwell et al. 2020; Paris 2008; Paris et al. 2022) and Lamanai (Simmons et al. 2009; Simmons and Shugar 2013a, 2013b). However, copper-based minerals such as malachite were occasionally used for funerary masks (González Cruz 2011; Manrique-Ortega et al. 2020a) and pigments used on murals and ceramic vessels (Cheung et al. 2015; Houston et al. 2009; Hurst 2009; Magaloni et al. 1995; Miller et al. 2013).

The cultural importance of greenstone in Ancient Mesoamerica

Greenstone objects have a very long history as precious objects in Mesoamerica. The use of greenstone offerings, including celt caches, dates back to the Early Formative period Olmec sites such as San Lorenzo and El Manatí (Clark and Coleman 2014; Jaime-Riverón 2010; Ortiz and Rodríguez 2000), and proliferated through early political centers of southeastern Mesoamerica including La Venta (Clark and Coleman 2014; Diehl 2005; Drucker et al. 1959), Chiapa de Corzo (Bachand 2013; Gallaga Murrieta and Lowe 2018), Cascajal (Englehardt et al. 2020); Aguada Fénix (Inomata et al. 2020), Ceibal (Inomata et al. 2013), the Belize Valley (Powis et al. 2016) and many others, including monumental serpentine pavements and celt caches. Meanwhile, at small Middle Formative villages, jade beads were incorporated into the material culture of ordinary households as personal ornaments and funerary objects (Hammond et al. 1977:41, 1991). Greenstone beads were often placed in the mouth of deceased individuals, a practice linked to the cycle of death and rebirth (Hammond 1991; Hruby 2015). From the Late Formative through the Classic period, they were increasingly incorporated into dedicatory caches and the royal regalia of dynastic rulers, which ranged from beads, pectorals, earspools, and carved plaques to elaborate diadems, carved sculptures, and funerary masks (Aguilar-Melo et al. 2019; Filoy Nadal 2010; Freidel et al. 2002; González Cruz 2011; Hammond et al. 1977:41; Juárez-Rodríguez et al. 2018; Manrique-Ortega et al. 2020a; Manrique-Ortega et al. 2020b). By Spanish Contact, greenstone beads were commonly used as currency items (Landa and Gaspar Antonio Chi [1581] in Tozzer 1941:94–96, 231) and objects forming part of imperial tax payments (Berdan and Anawalt 1992) as well as personal ornaments and ritual objects, with the former practice potentially dating back to the Late Formative period in the Maya Lowlands (Freidel et al. 2002). Masson and Freidel (2012:476) suggest that greenstone objects formed a continuum of value from small beads to polished jade celts, where items such as beads and serpentine axes were accessible to households across the socioeconomic spectrum (see also Freidel and Reilly 2010; Lesure 1999). Greenstone beads and objects were frequently given to the Spanish during attempts at early diplomatic relations (see summary in Foshag 1957:10–11).

Jade objects were produced through extensive carving, drilling and polishing techniques (Hruby 2015; Kovacevich 2006, 2013; Kovacevich and Callaghan 2019; Pendergast 1998; Rochette 2009). Evidence for concentrated lapidary productive activities has been identified through the presence of production debitage such as percussion flakes, sawn fragments, blanks, and tools such as abrader/polishers (Kovacevich 2006; Kovacevich and Callaghan 2019; Rochette 2009). These items are present at multiple sites in the Middle Motagua Valley in the San Agustín Acasaguastlán area (Smith and Kidder 1943; Rochette 2009) as well as at the site of Cancuen, a monumental zone strategically situated along the important south–north trade corridor that included the Río Pasión (Andrieu et al. 2014; Kovacevich 2006).

By the Late Postclassic period, greenstone was called *chalchihuitl* by Nahuatl-speaking peoples (Berdan and Anawalt 1992; Melgar Tísoc et al. 2018), specified as being the property of nobles, with particularly fine examples bearing the name of *quetzalitzli* (Sahagún 1963, Book 11:221–223). Book 11 of the Florentine Codex also lists a number of related stones, including *quetzalitzepyllotli* (a type of greenish-white jade; highly esteemed), *tlilayotic chalchihuitl* (greenish black; very expensive), *iztac chalchihuitl* (white jade with green and light-blue spots), and *mixtecatetl* (a mixture of white, black, and green, not esteemed; “the last of the green stones”) suggesting that the Aztecs had an extremely strong understanding of the range of color variation in jadeite and related minerals, which they ranked in value according to their characteristics (Sahagún 1963, Book 11:226). Book 9 of the Florentine Codex lists *chalchihuitl* and *quetzalitzli* as high-value commodities traded by the *pochteca* from the time of the second ruler, Tlacateotl, together with quetzal feathers, also a Maya highland product (Sahagún 1959, Book 9:1). Some of the greenstone obtained by the Aztec Empire was likely from the Gulf Coast, obtained through the trading missions of vanguard merchants to the Gulf Coast. These missions are described in some detail, mentioning that the Aztec merchants specifically visited the cities of Xicalanco, Cimatlan [Cimatán] and Coatzaqualco, and the rulers who governed them, and received “the large green stones, round, green, like tomatoes; the cylindrical green stones; then the green stones cut on a bias; the well-colored precious green stone which we call today the finest emerald-green jade; and fine bottle-green jadeite, and turquoise mosaic shields, and stones with green pyrites in their midst” (Sahagún 1959, Book 9:19). Other greenstone objects were obtained directly from outlying provinces through tax/tribute payments. *Chalchihuitl* was among the goods taken in tax payments from the imperial provinces of Soconusco (Pacific Coastal Chiapas) as well as a number of other provinces with which greenstone was exchanged including areas within the present states of Puebla, Guerrero, Oaxaca, and Veracruz (Berdan and Anawalt 1992; Nuttall 1901:229; Smith 1996:147). Additionally, Carmack (1981:142) suggests that the highland Guatemalan Maya political capital of K’umarkaj (Utatlán) formed a tributary relationship and marriage alliance with the Aztec Empire in 1510, where the rulers of K’umarkaj paid the Mexica in quetzal feathers, gold, precious stones (likely jade), cacao, and cloth. Notably, as Taube and colleagues (2004:205) observe, both the traded pieces from Xicalanco and the taxed goods from the provinces represent finished carved objects, mostly beads and plaques, rather than freshly quarried material. However, a small number of partially worked jade plaques and mosaic pieces recovered from the Templo Mayor (Melgar Tísoc et al. 2018) suggest that some jade ornaments were exchanged as preforms, blanks, or nodules, and worked into their final form in cities such as Tenochtitlan, as described in historical accounts of skilled lapidaries by Sahagún (1959:80–81).

The potential for greenstone sources in highland Chiapas

As early as 1901, Zelia Nuttall hypothesized that jadeite sources could be located in highland Chiapas (1901:228–229). She noted

that the Florentine Codex describes the native prospecting and mining of jade in its natural setting in significant detail (Sahagún 1963, Book 11:221–222), and noted the significance of the name of the modern/historic Chiapas town of Chalchihuitán, a Nahuatl toponym that translates as “The Land of *Chalchihuitl* [greenstone]” (Nuttall 1901:232). Recently, Taladoire (2016:15) reports several personal communications with scholars hypothesizing possible sources in this area. He notes the relative scarcity of jadeite objects at Tonina compared to Palenque, Yaxchilan, and Cancuen, hypothesizing the latter sites had greater access to Motagua jade via trade along the Usumacinta River, prompting Tonina to seek greenstone resources within the western Chiapas highlands (Taladoire 2016:15).

The modern town of Chalchihuitán sits within a broader regional system of left-lateral reverse and strike-slip faults known as Chiapas Fold and Thrust Belt, which runs roughly parallel to the Motagua–Polochic Fault System (Hernández-Vergara et al. 2021; Mora et al. 2007). This regional fault system extends from the Isthmus of Tehuantepec into central and northwest Chiapas, and is responsible for the creation of the Chiapanecan Volcanic Arc that punctuates the Central Highlands as far as El Chichonal Volcano in northwest Chiapas (Hernández-Vergara et al. 2021; Mora et al. 2007). The town of Chalchihuitán sits on the southern edge of the Tecpatán–Ocosingo fault, one of the principal east–west reverse faults of the system (Hernández-Vergara et al. 2021; Mora et al. 2007). Although this region has been minimally studied, we hypothesize that this fault could plausibly have created geological conditions similar to those of the Motagua–Polochic Fault System. The fault zone immediately to the south, the Telestaquín–San Cristóbal Fault, contains a segment that runs west–east from just north of San Cristóbal de Las Casas, through the town of Huixtán, to the town of Altamirano (Hernández-Vergara et al. 2021).

In 2017 and 2018, we visited local jewelers and market vendors in San Cristóbal de Las Casas, Chiapas, who reported to us that the greenstone objects that they sold were obtained from northwest Chiapas in the municipalities of Chalchihuitán and Chenalhó. Unfortunately, local armed conflicts during this time dispossessed large numbers of families from their homes, and also prevented us from traveling to these locations. Instead, we purchased small commercial samples from a number of vendors, asking them for the general provenience of each sample, and obtaining as much information as possible. In all cases where we purchased samples, the vendors told us that they obtained the raw materials second-hand, rather than quarrying or mining the materials themselves. A separate sample was collected from a road cut near the town of Huixtán, located approximately 30 km to the east of San Cristóbal de Las Casas. Below, we provide new mineralogical data on samples attributed to these source locations.

Materials

Archaeological samples

A total of 21 greenstone objects were identified from two sites in the Jovel Valley of highland Chiapas, Moxviquil

and CV-38, by the Proyecto Económico de Los Altos de Chiapas, directed by Paris and López Bravo. These sites represent the two largest monumental centers in the Jovel Valley (Figure 2); they were constructed principally during the Late Classic period, and remained occupied during the Early Postclassic period (Paris 2012). Moxviquil is located on the northern edge of the valley, and Cerro Ecatepec/CV-38 is located on its southwest corner. Cerro Ecatepec is positioned atop a steep limestone escarpment that includes linear mounds and masonry tombs (Culbert 1965). San Pedro y Pablo, or CV-38, is located on the valley floor below the escarpment, and included an I-shaped ballcourt and a concentration of public and residential architectural mounds (Aguilar 2005; Culbert 1965). Our excavations in 2009, 2015, and 2016 targeted residential architecture at both sites.

The sample of greenstone artifacts from these sites included beads in discoidal, tubular, and sculpted forms; ornament fragments; miniature manos; miniature axes; and a miniature effigy axe (Table 1; Figure 3). The objects range significantly in hue, including pale green, apple green, blueish green, and very dark green. Many of these objects, particularly the beads and ornaments, but also one of the miniature axe fragments (P7), were recovered from a funerary cave (Operation 7) located just below one of the residential hilltop zones in Moxviquil (Operation 4), where they likely served as funerary offerings and/or ornaments of the interred individuals. Most of the greenstone artifacts were recovered from contexts at the rear of the cave, and their original position may have been shifted due to the high level of post-depositional movement of remains and offerings, together with extensive modern looting and archaeological visitation by Frans Blom in the 1950s; we interpret them as offerings interred with the deceased individuals when they were placed in the cave (see Paris et al. 2020).

A number of other greenstone objects were recovered from both Moxviquil and CV-38. A small mano fragment (P20), two of the miniature axes (P17 and P19), and the effigy miniature axe (P18), were found in the Moxviquil Operation 4 residential zone (Paris et al. 2020). A fourth greenstone axe was found at CV-38 (P15). The three miniature axes are all between 5.0 and 6.1 cm in length, with damage to their distal ends suggestive of use, possibly in woodworking (P15, P17, and P19). Miniature axe P15 was recovered from a residential structure (Structure 10, Operation 3) at CV-38, and presents a flaring, convex bit with one corner heavily damaged from impact and striations on the tapered proximal end suggestive of hafting. Miniature axe P19 also exhibited significant usewear (micro-chipping and striations) on its convex distal edge, and was broken across the midsection. The axe was recovered from the lower levels of residential terrace fill adjacent to the remains of a domestic structure (Structure 8) together with ceramics and other objects dating to the Early Postclassic period (Paris et al. 2020). A second miniature greenstone axe (P17) was recovered from a nearby context associated with the structure fill of Structure 9, and also had significant damage on one corner, likely from use.

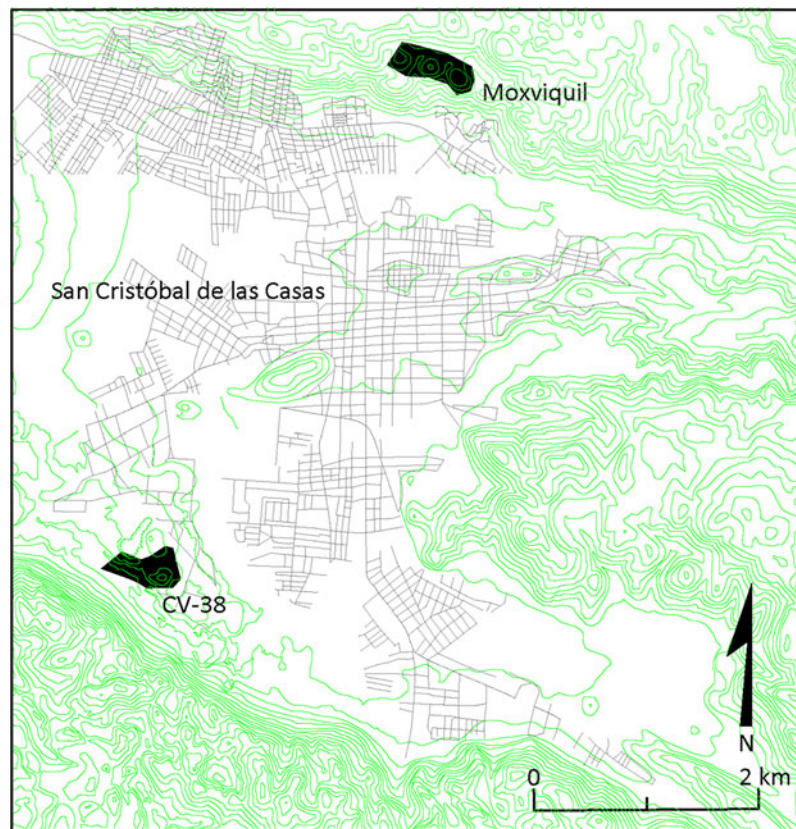


Figure 2. Map of the Jovel Valley. Drafted by Roberto López Bravo from Geodatos E15E52 and E15D62, INEGI.

However, the effigy miniature axe (P18), was too small to have actually been hafted, and analysis under a Dino-lite digital microscope indicated no evidence of usewear, suggesting that it was an effigy rather than utilitarian. We hypothesize that it was used as a type of currency (Paris and López Bravo 2021b). The effigy miniature axe was recovered from the western edge of the terrace that supported Structure 9 (Paris et al. 2020). The Moxviquil funerary cave and the CV-38 residence had occupations spanning the Late Classic and Early Postclassic periods, while the occupation at the Operation 4 residences was likely established in the Early Postclassic period (Paris et al. 2020).

Comparative samples

For comparative purposes, we collected 19 greenstone samples from local commercial vendors in both highland Chiapas and highland Guatemala, as well as an additional sample from a road cut near the town of Huixtán (Table 2, Figure 4). As mentioned above, due to local militarized conflicts during the study period, we were not able to collect greenstone samples from Chalchihuitán and Chenalhó in person. Samples were purchased from five locations: a local jeweler in San Cristóbal de Las Casas, an artisan market in San Cristóbal de Las Casas, a jeweler in Antigua, an artisan market in Guatemala City, and the local vendors at the Zona Arqueológica de Iximche to the west of Antigua. We conducted interviews with local jewelers and vendors to

determine the provenience of the sources to the best of their knowledge. The sources of the samples from San Cristóbal de Las Casas (SCLC) were consistently attributed to the neighboring municipalities of Chenalhó (SCLC artisan market) and Chalchihuitán (SCLC jeweler) in northwest Chiapas. The sources of the samples from the jeweler in Antigua were attributed to the Río Motagua while the vendors at the artisan markets in the Antigua and Guatemala City did not attribute their products to a specific source, though that would very likely also be somewhere in the Motagua Fault Zone. We intentionally purchased a range of colors, including everything from the apple-green color favored by the Classic period Maya, to the blueish-green color favored by the Olmec, as well as white, light green, mint green, dark green, and dark greenish black.

Methods

A number of methods have been used to characterize the composition and mineralogy of Mesoamerican greenstone in other studies. These include:

- 1) Detailed macroscopic mineralogy (Foshag 1957; Jaime-Riverón 2010; Manrique-Ortega et al. 2019; Manrique-Ortega et al. 2020b; Powis et al. 2016);
- 2) Petrography (Jaime-Riverón 2010; Jaime-Riverón et al. 2009; Lin et al. 2020; Powis et al. 2016);

Table 1. Jovel Valley greenstone archaeological specimens analyzed in the present study.

Specimen	Site	Op ^a	Cuadro ^b	Lot	Level	Capa ^c	Type	Length (mm)	Width (mm)	Thickness (mm)	Major elements, XRF ^d	Minerals, XRD ^e
P-1	Moxviquil	7	6-D	358	4	II	tubular bead	20	8	7	Al, Si, K, Ca, Fe	Paragonite (mica); maghemite
P-2	Moxviquil	7	6-C	357	3	I	discoidal bead	11	11	7	Al, Si, Ca, Fe	Jadeite
P-3	Moxviquil	7	6-C	357	3	I	carved bead	14	9	5	Al, Si, K, Ca	Jadeite
P-4	Moxviquil	7	6-D	352	3	I	tubular bead	18	8	7	Al, Si, K	Muscovite (mica)
P-5	Moxviquil	7	7-D	365	1	I	tubular bead	25	7	7	Al, Si, Ca, Fe	Omphacite
P-6	Moxviquil	7	5-C	363	1	I	tubular bead	14	6	6	Al, Si, K	Paragonite (mica); muscovite (mica)
P-7	Moxviquil	7	5-B	377	1	I	miniature axe	11*	19	7	Al, Si, Ca, Fe	Calcite; quartz; hematite
P-8	Moxviquil	7	6-D	349	2	I	discoidal bead	4	8	8	Al, Si, K, Ca, Fe	Muscovite (mica)
P-9	Moxviquil	7	5-B	383	1	I	tubular bead	16	7	7	Al, Si, K, Ca	Paragonite (mica)
P-10	Moxviquil	7	5-C	363	1	I	tubular bead	15	6	5	Al, Si, K, Ca	Ephesite; albite
P-11	Moxviquil	7	3-B	393	1	I	tubular bead	36	9	9	Al, Si, Ca, Fe	Omphacite
P-12	Moxviquil	7	7-D	367	3	II	discoidal bead	5	7	7	Al, Si, K, Ca	Diopside; calcite; grossular
P-13	Moxviquil	7	7-E	381	2	I	curved element	14	7	6	Al, Si, P, S, K, Ca	Anhydrite; alunite; kaolinite
P-14a	Moxviquil	7	6-C	357	3	I	asymmetrical bead	11	8	8	Al, Si, Ca, Fe	Jadeite; albite
P-14b	Moxviquil	7	6-C	357	3	I	tubular bead, short	9	7	7	Al, Si, K, Ca, Fe	Quartz; hedenbergite (pyroxene)
P-14c	Moxviquil	7	6-C	357	3	I	tubular bead, short	10	6	6	Al, Si, K, Ca, Fe	Grossular
P-15	CV-38	3	B-2	2	1	I	miniature axe	61	28*	16	Al, Si, Ca, Fe	Albite; quartz
P-17	Moxviquil	4	3-E	168	2	II	miniature axe	6	3.6	1.4	Al, Si, Ca, Fe	Jadeite, quartz; albite
P-18	Moxviquil	4	3-F	175	1	I	miniature effigy axe	24	24	11	Al, Si, Ca, Fe	Jadeite; omphacite
P-19	Moxviquil	4	19	254	4	I	miniature axe	55	29	25	Al, Si, Ca, Fe	Quartz; albite
P-20	Moxviquil	4	17	243	2	I	rectangular mano	*66	*46	*14	Al, Si, Ca, Fe	Quartz; albite

^aop = operation; ^bcuadro = unit; ^ccapa = cultural level; ^dXRF = X-ray fluorescence spectrometry; ^eXRD = X-ray diffraction; * = measurement of damaged or broken artifact.

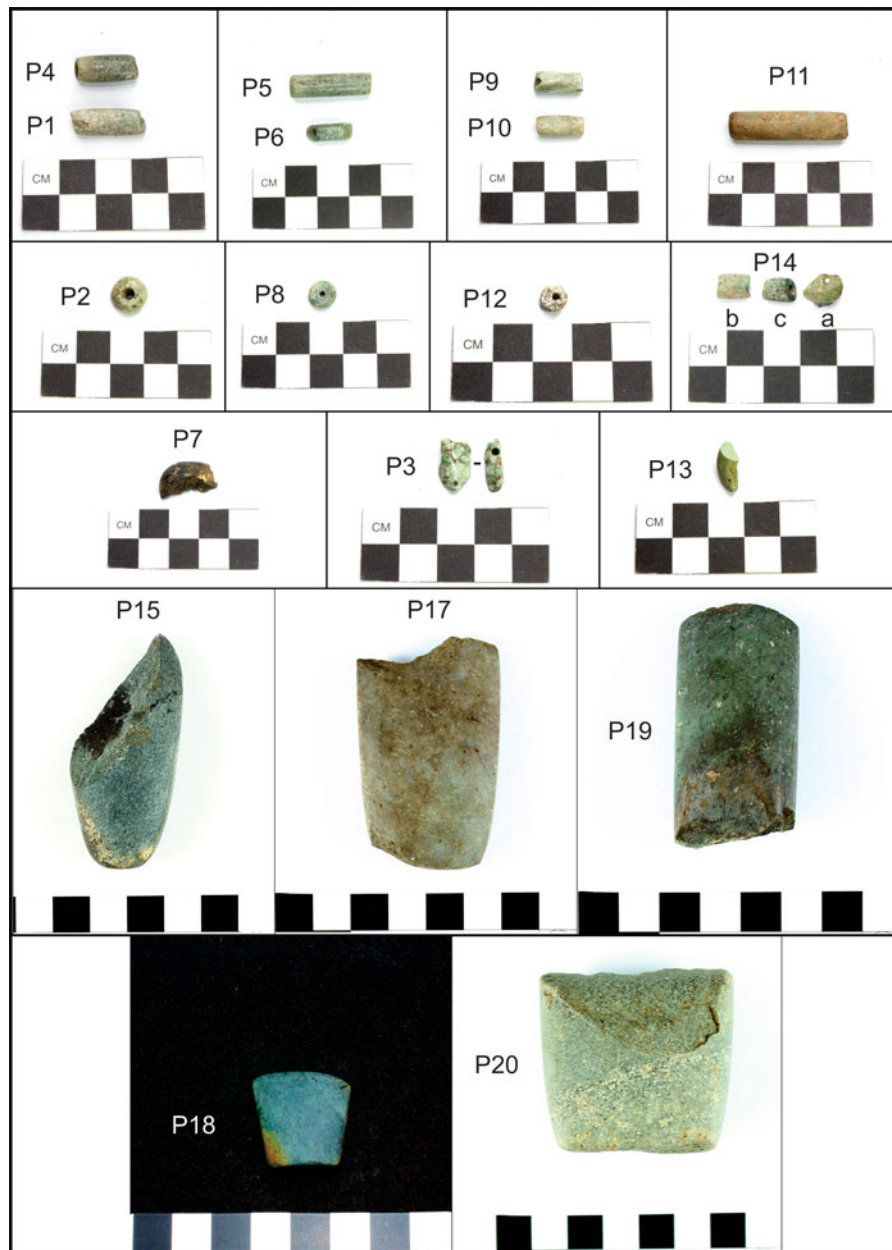


Figure 3. Jovel Valley greenstone archaeological specimens analyzed in the present study. Photos by Elizabeth Paris.

- 3) XRF (Aguilar et al. 2019; Aguilar-Melo et al. 2019; Delgado Robles et al. 2015; Englehardt et al. 2020; Hauff 1993; Hernández-Murillo et al. 2022; Juárez-Rodríguez et al. 2018; Knight et al. 2024; Manrique-Ortega et al. 2014; Manrique-Ortega et al. 2019; Manrique-Ortega et al. 2020b; Melgar et al. 2012; Ruvalcaba et al. 2011);
- 4) μ -XRF mapping (Lin et al. 2020);
- 5) XRD (Aguilar et al. 2019; Aguilar-Melo et al. 2019; Bishop et al. 1993b; Foshag 1957; Harlow et al. 2011:369; Hauff 1993; Jaime-Riverón et al. 2009; Knight et al. 2024; Lin et al. 2020; Manrique-Ortega et al. 2020b; Ruvalcaba et al. 2011);
- 6) Scanning Electron Microscopy with Energy Dispersive Spectroscopy (SEM/EDS) (Harlow et al. 2011:369; Jaime-Riverón et al. 2009; Knight et al. 2024; Manrique-Ortega et al. 2019; Manrique-Ortega et al. 2020b; Melgar Tísoc et al. 2018);
- 7) Electron probe microanalysis (Lin et al. 2020);
- 8) Inductively Coupled Plasma Mass Spectrometry (ICP-MS) (Healy et al. 2018; Kovacevich et al. 2005);
- 9) Neutron Activation Analysis (NAA) (Bishop et al. 1985; Bishop et al. 1993a; Bishop et al. 1993b, Hammond et al. 1977; Jaime-Riverón et al. 2009);
- 10) Particle-Induced X-ray Emission (PIXE) (Jaime-Riverón et al. 2009; Manrique-Ortega et al. 2019; Ruvalcaba et al. 2008; Ruvalcaba et al. 2011);
- 11) Raman Spectroscopy (Aguilar-Melo et al. 2019; Bernard et al. 2022; Delgado Robles et al. 2015; Gendron et al. 2002; Hernández-Murillo et al. 2022; Knight et al. 2024; Lin et al. 2020; Manrique-Ortega et al. 2014;

Table 2. XRD analysis results for comparative specimens from highland Chiapas and Guatemala.

Sample	Purchase location	Attributed source	Munsell	Color	Mineralogy
J1	Jeweler, SCLC	Chalchihuitán	5BG 5/2	Grayish blue green	Omphacite
J2	Jeweler, SCLC	Chalchihuitán	5 G 6/1	Greenish gray	Jadeite; quartz
J3	Jeweler, SCLC	Chalchihuitán	5 G 6/1	Greenish gray	Jadeite
J4	Artisan market, SCLC	Chenalhó	5 G 3/2, 5BG 5/2	Dusky green, grayish blue green	Antigorite (serpentine); hematite
J5	Artisan market, Antigua	Motagua RV	5BG 3/2	Dusky blue green	Omphacite; diopside
J6	Artisan market, Guatemala City	Motagua RV	5 G 5/2, 10 G 6/2	Grayish green, pale green	Jadeite; albite
J7	Artisan market, Guatemala City	Motagua RV	10 G 6/2, 5 G 6/1	Pale green, greenish gray	Jadeite; quartz
J8	Artisan market, Guatemala City	Motagua RV	5 G 2/1	Greenish black	Jadeite; omphacite
J9	Artisan market, Guatemala City	Motagua RV	5 G 2/1	Greenish black	Jadeite
J10	Jeweler, Antigua	Motagua RV	N7, N8	Very light gray, light gray	Jadeite; hematite; quartz
J11	Jeweler, Antigua	Motagua RV	5 G 5/2, 10 G 6/2	Grayish green, pale green	Omphacite; dolomite; maghemite
J12	Jeweler, Antigua	Motagua RV	5 G 5/2	Grayish green	Jadeite; quartz; hematite
J13	Jeweler, Antigua	Motagua RV	5 G 3/2, 5BG 5/2	Dusky green, grayish blue green	Omphacite
J14	Jeweler, Antigua	Motagua RV	5BG 3/2	Dusky blue green	Jadeite
J15	Jeweler, Antigua	Motagua RV	N3	Dark gray	Omphacite; quartz; hornblende?
J17	Artisan Market, Iximche	Motagua RV	5 G 2/1	Greenish black	Omphacite; kosmochlor(?)
J20	Road cut	Huixtán	10 GY 5/2, 5 G 5/2, 5 BG 5/2	Grayish green, grayish blue green	Lizardite (serpentine); hematite
Chenalhó round	Artisan market, SCLC	Chenalhó	5GY 3/2	Dusky green	Antigorite (serpentine)
Chenalhó square	Artisan market, SCLC	Chenalhó	5GY 5/2, 5GY 3/2	Dusky yellow green, grayish olive green	Antigorite (serpentine); hematite
Chenalhó teardrop	Artisan market, SCLC	Chenalhó	10 G 4/2, 5 G 3/2	Grayish green, dusky green	Antigorite (serpentine)

Notes: XRD = X-ray diffraction; SCLC = San Cristóbal de Las Casas; RV = River Valley. For mottled samples, the dominant color is listed first.

- Manrique-Ortega et al. 2019; Manrique-Ortega et al. 2020b; Melgar et al. 2012; Melgar Tísoc et al. 2018; Ruvalcaba et al. 2011; Smith 2005; Smith and Gendron 1997);
- 12) Fourier Transform-Infrared Spectroscopy (FT-IR) (Aguilar-Melo et al. 2019; Delgado Robles et al. 2015; Hernández-Murillo et al. 2022; Manrique-Ortega et al. 2014; Manrique-Ortega et al. 2020b);
 - 13) Visible and Near-Infrared Spectroscopy (VNIR) (Curtiss 1993; Hauff 1993);
 - 14) Cathodoluminescence (Lin et al. 2020);

As described below, our study uses a combination of XRF and XRD techniques. XRF is measured in weight-percent to 10 significant digits for the Bruker Tracer IV-SD calibrations used, so is not as sensitive as some other techniques such as ICP-MS and INAA, which typically measure in ppb or even up to 0.1 ppt; however, the advantages of XRF and XRD include the fact that they can be carried out both non-destructively and relatively rapidly (see Aguilar et al. 2019). When combined, they permit the consideration of both elemental and mineralogical composition (Aguilar et al. 2019; Aguilar-Melo et al. 2019; Lutterotti et al. 2016; Mendoza

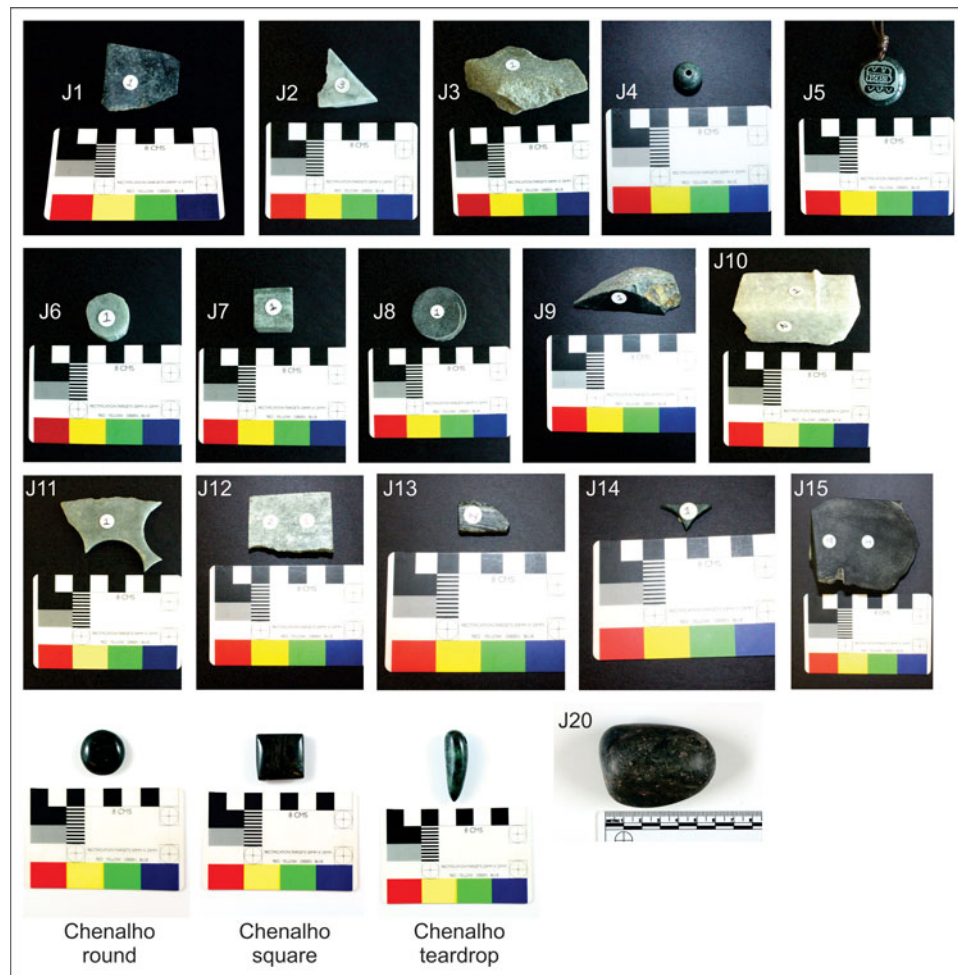


Figure 4. Comparative greenstone specimens analyzed in the present study. Photos by Elizabeth Paris.

Cuevas and Velázquez Maldonado 2015). As many scholars have noted, many “jade” objects are heterogeneous, with internally variable composition and with multiple minerals within a solid-state matrix (Bishop 2014:259; Manrique-Ortega et al. 2020b; Ruvalcaba et al. 2011). Techniques targeting mineralogy, such as XRD and Raman Spectroscopy, are critical for assessing greenstone object composition, and may be complimented by elemental techniques such as XRF, PIXE, INAA, ICP-MS, or SEM/EDS.

X-ray fluorescence

The chemical analysis was conducted by Paris at the University of Calgary, using a Bruker Tracer IV-SD (EDXRF) portable X-ray fluorescence spectrometer, with a silicon drift detector (SDD), Rhodium (Rh) target X-ray tube, a 3 x 4 mm x 7.5 µm beryllium window, and detection at rates of up to 200,000 ct/s. Instrument calibration was verified using the standard sample for the instrument provided by Bruker. Each sample location was analyzed twice: once using the Major Elements setting (15 kV, 35 µA, no filter, 180 s) and once using the Trace Elements setting (40 kV, 16.5 µA, Filter 1, 60 s). The empirical calibrations for these settings were developed by Bruker specifically to analyze

geological materials of uncertain and variable composition such as sedimentary rocks or ceramics (the full list of elements is specified in Supplemental Tables S2.1 and S2.2). Trace-element settings using Filter 1 (an Al/Ti alloy of 300 µm/25 µm) and higher voltage allow for a more accurate quantification of higher-Z elements, with an automated timer and with a tabletop stand to allow for precise measurements. The results were interpreted using the analytical software provided for the instrument, using the empirical calibrations for these settings developed by Bruker, displayed in weight-percent (wt%). Each sample was placed on the sample window in order to maximize accuracy, using flat facets, smooth surfaces, and full contact where possible to minimize reflectance (see Hernández-Murillo et al. 2022). Bruker’s documentation for the instrument states that the limit of detection (LOD, defined as the level of concentration at which the presence of an element in a sample can be detected above background) is 3σ as measured on a test blank.

As noted previously, the samples were analyzed using XRF spectrometry of unmodified artifact surfaces. Elemental concentrations represent bulk chemistry measurements within the approximately 3 x 4 mm spot area, with depth of

penetration varying for measured elements as a function of photon energy and material density. As previously mentioned, many “jade” objects are heterogeneous, with internally variable composition, and multiple minerals within a solid-state matrix (Bishop 2014:259; Manrique-Ortega et al. 2020b; Ruvalcaba et al. 2011); thus, depending on the sample location, any given XRF measurement may represent multiple mineral grains, and internal variation within samples is expected. For the Chenalhó square sample, 10 locations were analyzed in a quincunx formation on both sides of the sample; the results suggests relatively low variation in trace-element concentrations, and slightly greater variation in major element concentrations of Mg, Si, and Fe, although even for these elements, the coefficient of variation remained under 2 (Supplemental Table S1.1, Supplemental Figure S1.1). Mg and Si are two of the principal elements in serpentinite ($Mg_6[Si_4O_{10}](OH)_8$), suggesting that this variation is due to variation in beam placement with respect to individual mineral grains. Heterogeneous composition can be partially offset by using a larger spot size, and by pairing XRF with other nondestructive techniques such as XRD or elemental surface mapping to identify heterogeneous mineralogy within individual samples.

The exterior surfaces and edges of the objects were also examined and imaged using a Dino-lite digital microscope at 40x.

X-ray diffraction

The greenstone pieces were also analyzed by Meanwell at the Massachusetts Institute of Technology by XRD. XRD uses X-rays to detect the reflections of specific crystal planes within the sample. This technique allows for the identification of crystalline mineral phases, which is not always possible through chemistry alone, particularly when multiple minerals are present in the same sample. Most of the smaller artifacts and reference specimens were analyzed in the Bruker D8 with a General Area Detector Diffraction System (GADDS) using a Cobalt (Co) $K\alpha$ X-ray source ($\lambda = 1.7190 \text{ \AA}$) at 35 kV and 40 μA and a two-dimensional (2-D) detector. The Co source is particularly useful for analyzing samples that contain iron, like many of the greenstone samples, because the wavelength of Co incident X-rays does not cause fluorescence from iron unlike a Cu X-ray source (Henry et al. 2022). The 2-D detector measures a portion of the Debye ring which can then be analyzed for inhomogeneities that result from oriented crystal grains in a sample, such as is the case for many polycrystalline geological samples (Flemming 2007). The diffraction patterns can also be examined for oval rings that indicate that the crystallites are stressed (He et al. 2002). The samples were scanned through a 2-theta angle range of 15° to 80° in three frames with 120 s exposure time per frame, and the samples were also continually oscillated during the scan so that an approximately 1 mm² area of the sample was exposed to the radiation, thus hopefully avoiding sampling only one mineral grain.

Two of the greenstone pieces (P19–20) were too thick to be placed in the Bruker D8 instrument, which requires a

certain distance between the X-ray source and the sample. These pieces were instead analyzed in the Rigaku SmartLab XRD using a Cu $K\alpha$ X-ray source. These were scanned through a 2-theta range of 0° to 90°. This machine is not equipped with a moving stage, so only a small spot was analyzed, although the broadest beam focus was used to attempt to analyze as large an area as possible. The Huixtán roadcut specimen (J-20) and reference sample J-15 were also analyzed in a different instrument, the PANalytical X’Pert with a Mo X-ray source, due to instrument availability.

After the data was collected, the diffraction patterns were integrated across the area of the 2-D results and the resultant peaks were imported to HighScore Plus to complete the phase identification. For each sample the background was removed and peaks were automatically detected and refined by hand. These peaks were compared to reference patterns of various minerals. In most cases, one to three mineral phases were clearly present, and occasionally one or more peaks were left unidentified. These peaks cannot be linked definitively to a specific mineral phase without additional peaks from that mineral.

Results

Jovel Valley specimens

In general terms, the archaeological greenstone specimens can be separated into a jadeite group ($N = 8$), a micaceous group ($N = 7$), and specimens that have a unique mineralogy within the sampled specimens ($N = 6$; Table 1, Figures 5 and 6, Supplemental Tables S2.1 and S2.2, Supplemental Figures S1.9–50, S1.134–154). Specimens in the jadeite group contained at least one of the jade-associated pyroxene minerals, including jadeite, omphacite, and diopside, along with potential accessory minerals. These included a diverse range of objects, including one of the miniature axes (P17), miniature effigy axe (P18), tubular beads (P5, P11), discoidal beads (P2), asymmetrical beads (P14a), and a bead carved in a shape that may be the stylized head of a feline (P3, see Figure 5a). Comparisons between the XRF (Supplemental Figures S1.9–S1.133) and XRD (Supplemental Figures S1.134–154) results indicated that the majority of the jadeite specimens lack potassium (Supplemental Table S2.1), which is commonly characteristic of muscovite mica. The only specimen within the jadeite group with a high potassium signal was the sample of diopside also containing calcite and grossular (green garnet; P12). The pyroxene minerals are significantly harder and denser than micas, which makes them harder to shape into the desired form, but results in finished objects that are significantly more durable. The identification of minerals frequently associated with jadeite deposits (albite, quartz) is unsurprising due to the metamorphic environment in which jadeite is formed. Notably, the XRF results indicated an absence of magnesium despite high calcium peaks (Supplemental Table S2.1) although significant magnesium concentrations were noted in the comparative Chenalhó samples, suggesting it is not a detection issue. This is unexpected because both elements are typically

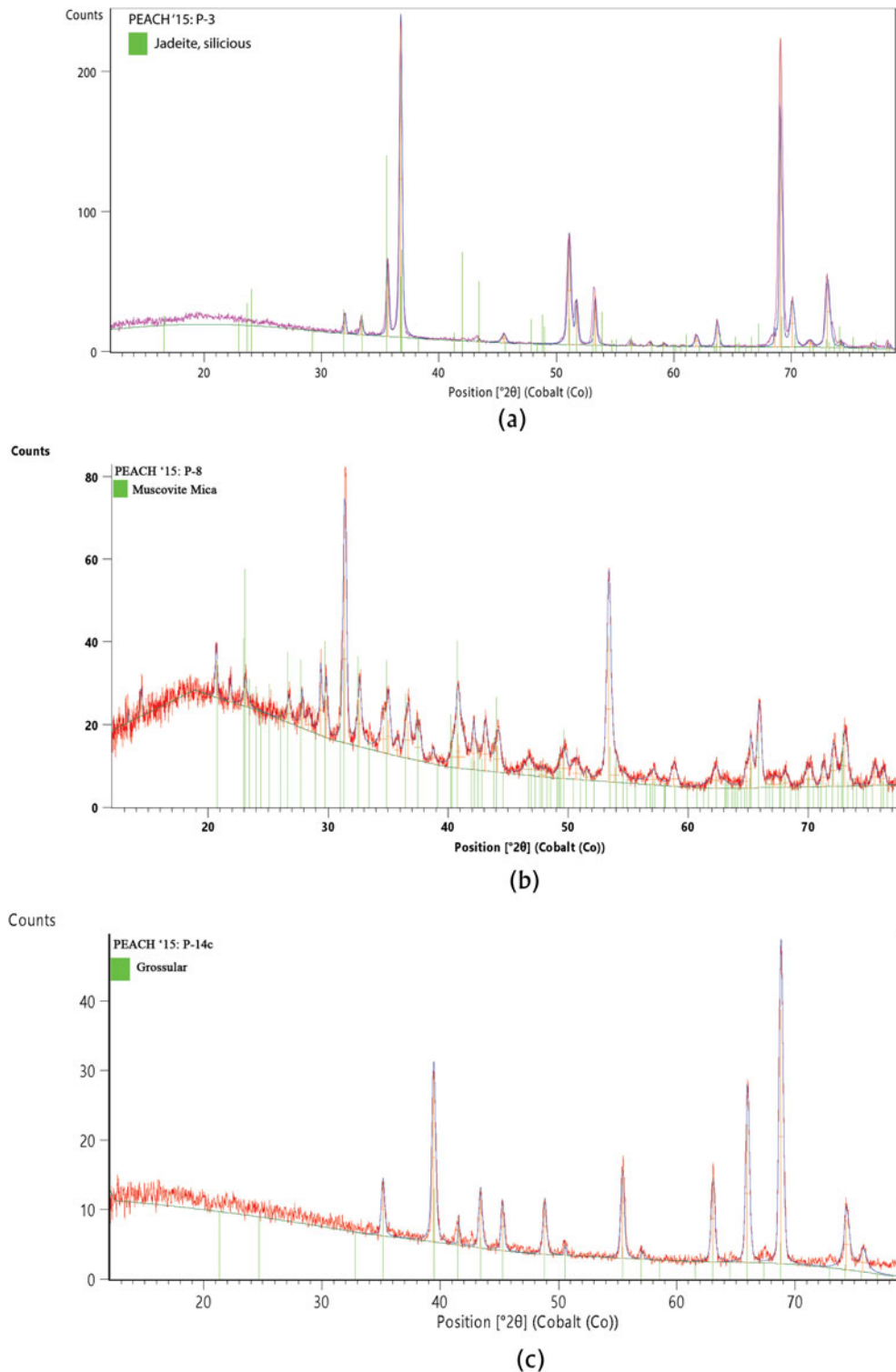


Figure 5. Selected XRD diffraction patterns showing: (a) a jadeite group sample (artifact P-3), with the reference spectrum for jadeite; (b) a micaceous group sample (P-8), with the reference peaks for muscovite mica; and (c) the sample containing grossular (P-14c) with the reference peaks for grossular showing excellent agreement.

present in diopsides and many of the other materials found in the metamorphic environments associated with jadeite deposits, such as chlorite, soapstone, serpentine, dolomite, olivine, and monticellite.

Several different types of micas were identified within the micaceous group, principally muscovite, paragonite, and ephesite. All of these objects were beads from the Moxviquil funerary cave, and they were often visually

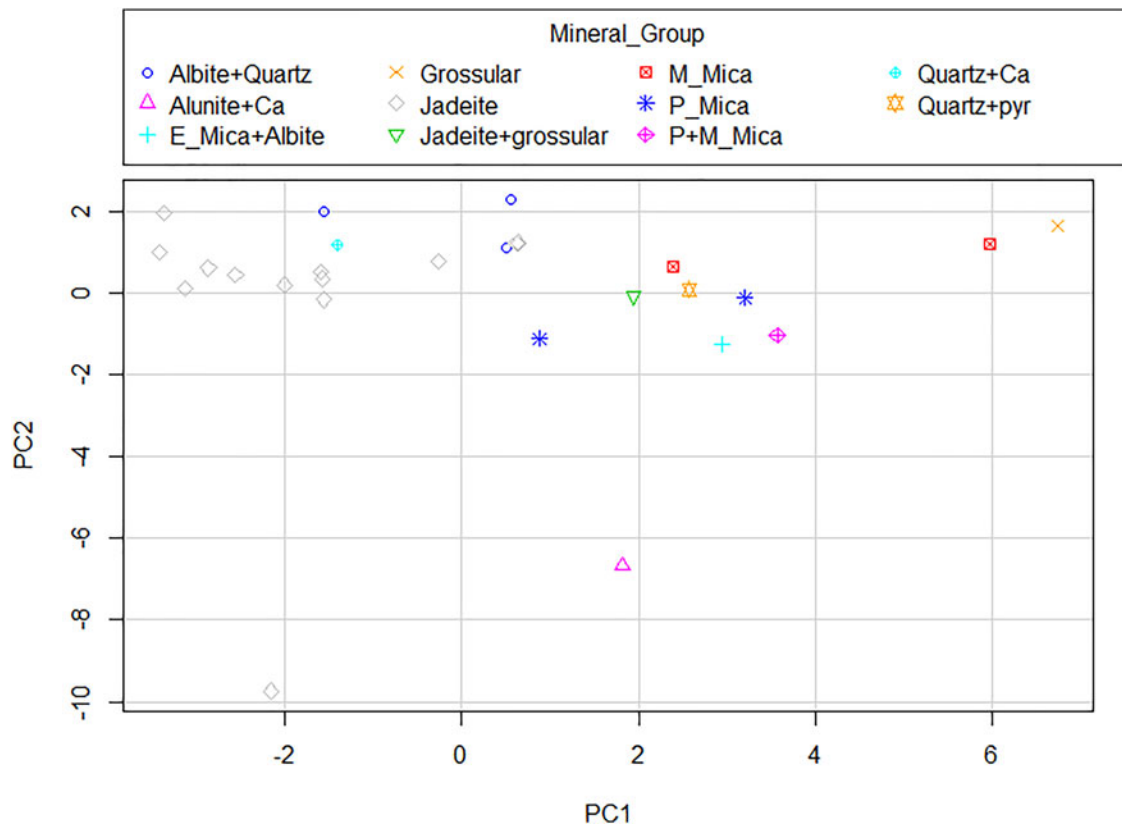


Figure 6. Principal components analysis (PCA) of Jovel Valley greenstone specimens (majors and traces), classified by mineral group. Jadeite group includes jadeite, omphacite, and diopside minerals; see Table 1. Paragonite mica (P_mica), muscovite mica (M_mica) and ephesite mica (E_mica) are differentiated. See Supplemental Tables S1.2, S1.3.

distinctive from the jadeite group, with a sparkly luster; some specimens also displayed a foliated crystal habit that is often characteristic of micas. Several of the samples identified through XRD as muscovite also had high potassium values as observed in XRF results (Supplemental Table S2.1). Artifacts containing muscovite mica included tubular beads (P4, P6, see Figure 5b) and discoidal beads (P8), while samples containing paragonite mica included tubular beads (P1, P6, and P9). Only one tubular bead contained ephesite (P10). Some of the samples from the micaeous group also contained other minerals, such as maghemite ($(\text{Fe}_{0.67}\square_{0.33})\text{Fe}_2\text{O}_4$), P1), green quartz (SiO_2 ; P14b), and albite ($\text{Na}(\text{AlSi}_3\text{O}_8)$; P10).

The last group of samples contained a range of other green minerals. One of the small tubular beads (P14c) was produced from a dark greenish-blue grossular, a type of green garnet (Figure 5c); this mineral was also found in discoidal bead P12, together with diopside and calcite. The miniature axe fragment from the funerary cave (P7) was a mixture of dolomite, quartz, and hematite, and was a dark greenish black in color. Notably, it was not classified as chloromelanite as per other archaeological specimens of a similar color (e.g. Foshag 1957:23). The small, irregular, projection-like sample (P13) has a highly distinctive composition which includes aragonite (CaCO_3), calcium sulfate (CaSO_4) and alunite ($\text{KAl}_3(\text{SO}_4)_2(\text{OH})_6$). The XRF spectrum for this sample also contains sulfur; it the only sample

that has sulfur as one of the major elements, which is consistent with this mineralogy (Supplemental Tables S2.1 and S2.2). Sample P13 also has a very fine granular texture, which was different from the other green stones analyzed. Finally, one of the miniature axes (P19) and the miniature rectangular mano fragment (P20) contained quartz and albite feldspar (see Table 1). As mentioned above, albite is a common sodium feldspar that occurs in association with micaceous and jadeite samples. It generally has a grayish or whitish tone, but may appear greenish with iron impurities; Sample P20 appears mint green in color.

Finally, the absence of copper in XRF or XRD diffraction patterns of copper minerals confirms that the archaeological specimens do not contain malachite, turquoise, or other copper-based minerals.

Comparative specimens

In general terms, the comparative greenstone samples contain a range of minerals that include minerals from the jadeite group ($N=15$), antigorite/lizardite (serpentinite; $N=5$) (see Table 2; Supplemental Tables S1.4, S1.5, S2.3, S2.4, Supplemental Figures S1.2, S1.3, S1.51–133, S1.155–S1.174). All three specimens attributed to Chalchihuitán were characterized as jadeite/omphacite. The four specimens attributed to Chenalhó were all characterized as serpentinite (antigorite), with a high wt% Fe in the XRF results (Supplemental

Table S2.1; Supplemental Figure S1.4). The high iron may be partially due to included hematite, which was seen in at least one of the XRD diffraction patterns. Notably, the jadeite samples attributed to Chalchihuitán included a range of colors, which we classified as forest green, mint green, and light green; while the Chenalhó specimens included a narrower range of colors including normal green and dark green. The roadcut specimen from near the town of Huixtán is very similar to the Chenalhó specimens, and is lizardite (serpentine).

The commercial specimens purchased in highland Guatemala were predominantly jadeite, and also included commonly associated minerals such as diopside, omphacite, albite, and quartz. Jadeite/omphacite samples presented a variety of colors, from white, to light green to apple green, to blueish green, to dark greenish black. These findings reinforce the need for compositional analysis in assessing mineralogy, as a reliance on color can be highly misleading.

XRF analysis suggests that there are some small trace-element compositional differences between Chiapas and Guatemala jadeite samples. For these tests, only trace elements were used to prevent duplication of sorting by mineralogy. MANOVA (multivariate analysis of variance; specifically Pillai's trace) was used to compare multivariate means of Guatemala and Chalchihuitán jadeite samples by group, performed on trace elements (CoKa1, NiKa1, CuKa1, ZnKa1, AsKa1, PbLa1, ThLa1, RbKa1, U.La1, SrKa1, Y.Ka1, ZrKa1, NbKa1, MoKa1, SnKa1, SbKa1) after eliminating one outlier identified through the principal components analysis (PCA) (J3.3). Pillai's trace statistic was 0.64382, with a

p -value of 0.0569, suggesting compositional overlap between the two groups, and a lack of statistical significance in the differences between the trace-element composition, but is only just above a significant probability value (Supplemental Table S1.6). Follow-up analysis examining the summary of the analysis of variance models for each element indicates that while concentrations of most elements are not significantly different, trace elements with significant p -values (below 0.05) include Zn, Sr, Nb, and Sb; however, there is still significant overlap in the distributions of the raw concentration values between the two groups (Figure 7; Supplemental Figures S1.5, S1.6, S1.7, and S1.8). The lack of significance in Pillai's trace and the overlap in the distributions does not currently allow us to assign geographical provenance to Jovel Valley archaeological specimens, whether composed of jadeite or of other minerals (Figure 8). While XRF and XRD are useful in providing a relatively detailed characterization of the specimens in our sample, we speculate that other methods are needed to differentiate between sources. Techniques that can measure heavier trace elements at ppb or ppt, such as INAA or ICP-MS, may be able to identify discriminating factors.

Discussion and conclusion

The Jovel Valley greenstone assemblage included green objects with a wide variety of mineralogies, which were often surprising with respect to their macroscopic characteristics such as color, texture, and luster. The artifacts

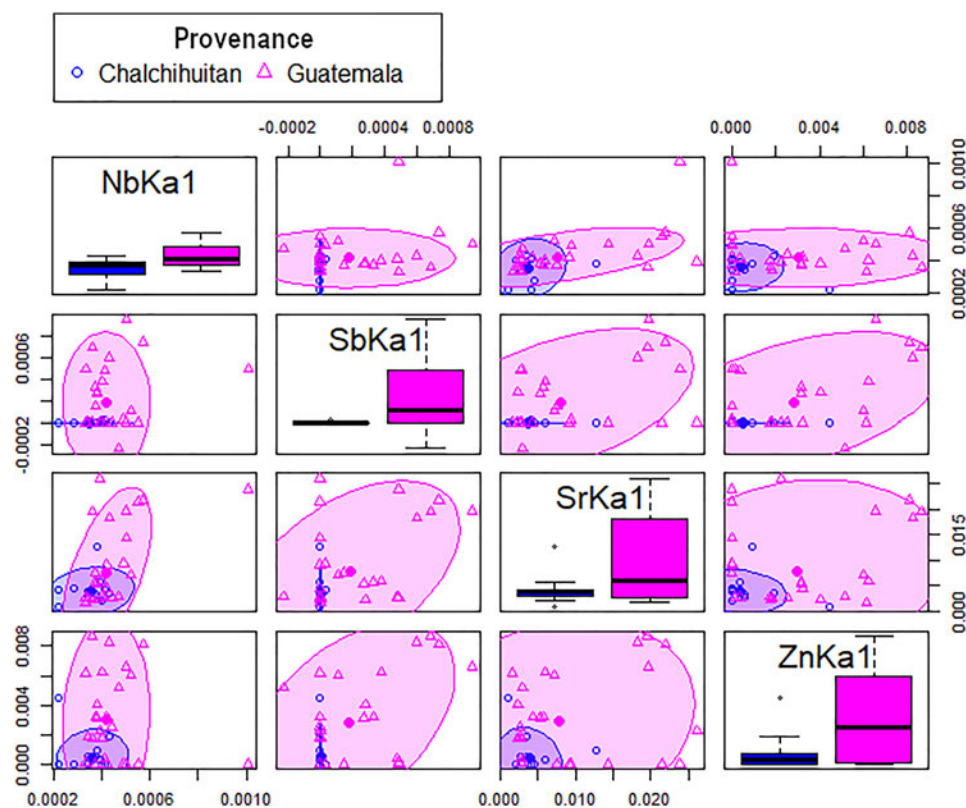


Figure 7. Scatterplot matrix of elemental concentrations for Nb, Sb, Sr, and Zn for jadeite comparative samples, by provenance group. Concentration ellipses are 0.95.

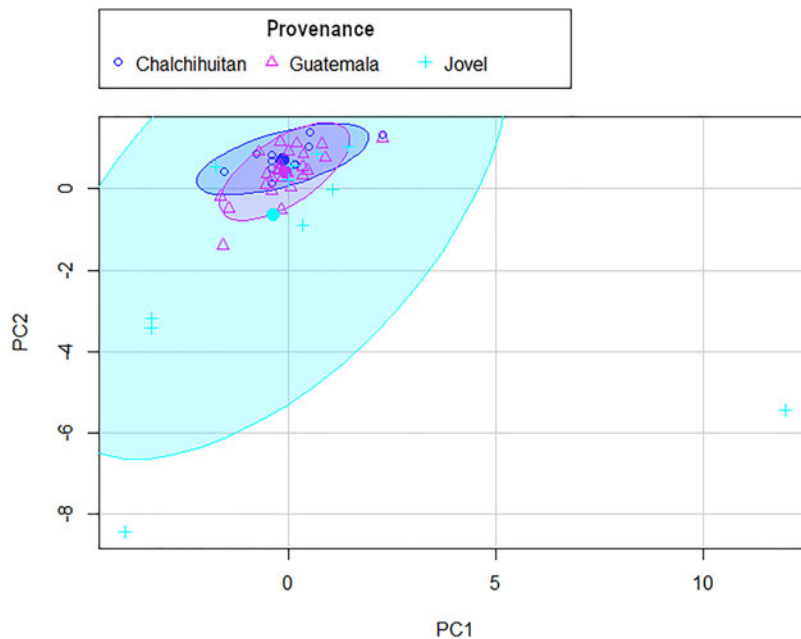


Figure 8. Principal components analysis (PCA) of trace elements of comparative and Jovel Valley jadeite specimens, classified by provenance. Concentration ellipses are 0.95. See Supplemental Tables S1.4 and S1.5.

included a jadeite group that contained a variety of pyroxene minerals, such as jadeite, omphacite, and diopside; a micaceous group, which included paragonite, muscovite, and ephesite; and a variety of other green minerals. Certain associations between form and mineralogy were noted; for example, the miniature axes and the mano were made out of quartz/albite. However, axes P17 and P18 also contained jadeite minerals, so this vague association is not statistically significant, given the sample size. Tubular and discoidal beads were made out of a wide range of materials, with similar dimensions, and all recovered from the Moxviquil funerary cave context. While jadeite is more valued today, we can speculate that the micaceous, grossular, and quartz beads may have come from the same deposit areas, and may have also been valued by Jovel Valley for their range of jadeite-like green colors. The limited number of greenstone artifacts recovered from Jovel Valley sites suggests that it was relatively rare and valuable. However, the fact that the miniature axes show evidence of usewear (with the exception of the effigy, P18), and were found in non-elite household midden contexts, suggests that high-value raw materials could also have utilitarian uses and were relatively accessible across the socioeconomic spectrum. The selection of mineral resources used for the axes may also be related to the fact that the axes appear to have been used, because quartz, albite, and jadeite/pyroxene are harder than micas. Grossular, however, is in the same hardness range as quartz.

If we assume (perhaps incorrectly) that many of the Jovel Valley greenstone items were imported from the Motagua rather than Chalchihuitán, our findings suggest a range of raw material sources, as would be expected for items received through long-distance exchange. For example, Harlow and others (2011:380), argue that none of the

jadeitites to the north of the Motagua Fault contain quartz, either as inclusions in jadeite or in veins, but all contain albite, mica, and usually analcime; while jadeites from south of the Motagua Fault frequently present quartz inclusions in jadeitite. However, many of the Jovel Valley specimens contain both albite and quartz, suggesting an unidentified source, either in the Motagua or elsewhere. Furthermore, the Jovel Valley micaceous specimens include both paragonite and muscovite, and specimen P6 includes both types, although paragonite is characteristic of the north Motagua and muscovite is more common in the south Motagua deposits. Minimally, we consider it very unlikely that a single location in the Motagua Valley supplied all of the greenstone items consumed by Jovel Valley sites.

Working towards a general assessment of a potential Chalchihuitán jadeite source, the mineralogy appears to have expected characteristics wherein jadeite specimens (attributed to Chalchihuitán) were recovered in close proximity to green antigorite (serpentinite) deposits (attributed to Chenalhó). Materials of both mineralogies displayed a range of colors, a characteristic also noted for the comparative Motagua samples. This suggests that as with the Motagua-Polochic Fault System, the proposed source locations in northwest Chiapas contain a range of minerals that includes both jadeites and serpentinites, likely with a small degree of geographic separation with respect to the locations of modern mining activity. At Chiapa de Corzo, Tomb 1 is one of the earliest elite funerary contexts in the region (750–700 B.C.), and contained 2,700 greenstone beads, including jadeite, antigorite, green quartz, and one turquoise specimen (Manrique-Ortega et al. 2014). Greenstone assemblages at large Classic period monumental zones in northeast Chiapas contain a diverse range of

transported westward via Chinkultic would likely have reached La Trinitaria (Zapaluta; Navarrete 1978), and from there would most likely have been transported westward across the Comitán Plateau and highland routes to the Jovel Valley. Jade and obsidian could also have been transported from highland Guatemala south through the Cuchumatanes Mountains via Zaculeu or Nebaj (Feldman 1978); then either north to the Comitán Plateau, or west via canoe along the Grijalva River to port towns such as Chiapa, Sitio Ruíz, or Acala, then to the Jovel Valley via overland routes (Navarrete 1978).

Chalchihuitán is equally plausible as a supplier of jadeite commodities to the Jovel Valley, via transportation routes connecting the Jovel Valley with Gulf Coast trading colonies in Cimatán (a Nahuatl-speaking trade colony on the Gulf Coast). Both Bernal Díaz del Castillo and Diego de Godoy, who took part in the 1524 siege of Chamula under Luis Marín, mention that the Spanish armies were led by their Zinacantán allies (just west of the Jovel Valley) to the Gulf Coast, by traveling north to Huitiupan (near Simojovel), then west to Tapilula, and then north again to the town of Ixtapangajoyá in Cimatán province; Bishop Bartolomé de Las Casas later passed along this route in reverse (Navarrete 1978; Viqueira 2006; Viqueira Albán 1999). Viqueira (2006) has hypothesized that parts of this route, called “Los Zoques” in the colonial period, may have been used by Aztec vanguard merchants for military incursions to secure transportation routes from their trade colonies in Cimatán, across highland Chiapas via Huixtán and Zinacantán, to the Soconusco province, evading Chiapa de Corzo and the portion of the Central Depression controlled by the Chiapanecs. Few details are available for the portion of the journeys between the Jovel Valley and Huitiupan. Still, the pre-Hispanic route may have passed from the Jovel Valley through Chamula, San Andrés Larrainzar, and the polity capital of Huixtán (today Santiago El Pinar), which is located about 8 km west of Chalchihuitán as the crow flies (Viqueira 2006:151). A second, less-traveled route from the Jovel Valley takes a slightly more easterly route, passing by the site of Moxviquil itself, to Chenalhó and Chalchihuitán, along smaller mountain roads. The end-point of both routes is Simojovel (just south of Huitiupan), location of the largest amber source in Mesoamerica, which formed part of the tribute demanded by the Aztec Empire from towns in the Soconusco (Navarrete 1978). Additional roads connected Tapilula north to piedmont towns such as Ixtacomitán, Solosuchiapa, Ixtapantajoyá, and Teapa in the Colonial period (and very likely in pre-Columbian times); Ixtacomitán was a major cacao production area (Wasserstrom 1983:38), and the band of cloud forest habitat between Tapilula and Teapa was well-known as quetzal habitat (Palacios 1928; Solórzano et al. 2003). Thus, overland trade routes connecting the Jovel Valley and Cimatán plausibly facilitated the transport of at least four high-value natural resources (greenstone, amber, cacao, and quetzal feathers). At the northern ends of these routes, Nahua merchants obtained greenstone items (particularly *quetzal-chalchihuitl*) and other Maya-area resources (Spondylus shell, tortoise shell, feathers, and animal pelts) at the

important trading centers of Xicalanco and Cimatán (Sahagún 1959:18)

The sample of archaeological specimens from Moxviquil and CV-38, while small, provides significant insights into the use and importance of greenstone objects for everyday households at the small polities that defined this region during the Late Classic and Early Postclassic periods, as well as new hypotheses concerning the trade routes that supplied them. These objects were personal adornments, funerary ornaments, currencies, and well-used tools, with green colors that connotated preciousness and high value. The chemical and mineralogical compositions of these objects suggest that they were crafted from a variety of stones, mostly available within the Motagua–Polochoic Fault System, and also possibly from newly described jadeite sources attributed to Chalchihuitán by our local contacts. More work is needed to characterize the range of minerals and their composition from this location, and the degree to which they were exploited in pre-Columbian times, and to perhaps reconsider potential trade routes and exchange relationships that may have connected highland Chiapas and its high-value raw materials with the broader Mesoamerican world.

Resumen en español

La piedra verde fue utilizada durante la época prehispánica en Mesoamérica para producir artículos de importancia cultural, como hachas, orejeras, figurillas y cuentas; objetos que se usaban a menudo para la acumulación de riqueza, y como adornos, símbolos de estatus y elementos preciosos en ofrendas y contextos funerarios. Los objetos eran fabricados de jadeíta, así como de otros minerales verdes a los que a menudo se hace referencia como “jade social.”

La presente investigación muestra las características mineralógicas de 21 artefactos de piedra verde recuperados en sitios del Valle de Jovel, Chiapas, México, para documentar la variedad de minerales verdes aprovechados por sus habitantes. Los artefactos fueron recuperados por el Proyecto Económico de Los Altos de Chiapas, dirigido por Paris y López Bravo, durante las temporadas 2009, 2015 y 2016. Los materiales provienen de una variedad de contextos; la mayoría fueron recuperados en una cueva funeraria en el sitio de Moxviquil, y el resto provienen de contextos domésticos en otros sitios a lo largo del valle. Los tipos de artefactos de piedra verde incluyen cuentas de forma discooidal, tubular y talladas; fragmentos de adornos; manos miniatura; hachas miniatura; y un hacha efígie miniatura.

El análisis composicional de los objetos sugiere que los mayas del Valle de Jovel del período Clásico Tardío (600–900 d.C.) y Posclásico Temprano (900–1200 d.C.) tuvieron acceso a una variedad de minerales de piedra verde, incluidas serpentinita, mica verde, grosularia y jadeíta. La caracterización de los objetos por XRD y XRF indica que las cuentas estaban hechas de una variedad de materiales, incluido jade/onfacita; micas como moscovita, paragonita y efesita; y grosularia (granate verde). Las hachas en miniatura estaban hechas de jade, dolomita y mezclas de albíta y cuarzo. La ausencia de cobre en los espectros XRF o

XRD confirma que los objetos arqueológicos no contienen malaquita, turquesa u otros minerales a base de cobre.

Para comprender mejor las posibles sitios de origen de los minerales, también analizamos muestras de referencia de la zona de falla Motagua-Polochic y fuentes vinculadas al área de Chalchihuitán-Chenalhó en Chiapas, México. Estas fuentes se compraron de proveedores locales, principalmente en la Ciudad de Guatemala, Antigua y San Cristóbal de las Casas, a quienes se entrevistó sobre su procedencia geográfica. Los especímenes comerciales comprados en las tierras altas de Guatemala eran predominantemente jadeíta y también incluían minerales comúnmente asociados como diópsido, onfacita, albíta y cuarzo. Dentro del área de Chalchihuitán-Chenalhó, especímenes de jadeíta (atribuidos a Chalchihuitán) parecen haber sido recuperados muy cerca de depósitos de antigorita verde (serpentinita) atribuidos a Chenalhó. La comparación sugiere que ambas áreas son regiones potenciales de fuente de materia prima de piedra verde utilizada en el Valle de Jovel, y que la asociación entre las micas y los minerales de jade sugiere la presencia de múltiples fuentes de materiales en la colección de artefactos.

Planteamos que los habitantes del Valle de Jovel tuvieron acceso a materiales intercambiados a larga distancia a través de rutas comerciales históricamente documentadas, que permitieron el movimiento de materiales de piedra verde desde el Valle del Río Motagua hacia las tierras altas de Chiapas al occidente, y posiblemente también desde el área de Chalchihuitán-Chenalhó hacia el sur. Las rutas comerciales terrestres que conectan el valle de Jovel con el área de Chalchihuitán-Chenalhó y el área de Cimatán de la costa del Golfo habrían facilitado el traslado de al menos cuatro recursos naturales de alto valor (piedra verde, ámbar, cacao y plumas de quetzal). Se necesita más trabajo para caracterizar la variedad de minerales y su composición del área de Chalchihuitán-Chenalhó, el grado en que fueron explotados en la época precolombina y tal vez reconsiderar posibles rutas comerciales y relaciones de intercambio que pueden haber conectado las tierras altas de Chiapas y sus alrededores con sus contemporáneos mesoamericanos.

Acknowledgments: We thank the Consejo de Arqueología, Instituto Nacional de Antropología e Historia (INAH) for permits granted to the Proyecto Económico de los Altos de Chiapas (2009) and Proyecto Interacción Entre Reinos en los Altos de Chiapas (2015), as well as permission to export and analyze the samples (Oficio 40.35.16-2018/1358). Funding for the 2009 season was provided by a National Science Foundation Doctoral Dissertation Improvement Grant (Award ID 0836590) to Paris to support fieldwork and lab analysis in 2009. Support for the 2015 excavations was provided by a Wenner-Gren Foundation International Collaborative Research Grant to Paris and López Bravo. We thank the University of Calgary, Universidad de Ciencias y Artes de Chiapas, ProNatura Chiapas, Museo Na Bolom, Centro INAH-Chiapas, the New World Archaeological Foundation, and our project staff and students. Many thanks also to the Center for Materials Research in Archaeology and Ethnology at MIT, and the Materials Research Laboratory at MIT, particularly Dr. Charles Settens and Dr. Jordan Cox. This work was carried out in part through the use of MIT.nano's facilities.

Competing interests: The author(s) declare none.

Data availability statement: Calibrated data for the XRF analysis of the reference samples and archaeological objects are included in the Supplementary Data files with this paper. The raw XRD spectra will be hosted on the *Ancient Mesoamerica* website.

Funding statement: Funding for the 2009 season was provided by a National Science Foundation Doctoral Dissertation Improvement Grant (Award ID 0836590) to Paris to support fieldwork and lab analysis in 2009. Support for the 2015 excavations was provided by a Wenner-Gren Foundation International Collaborative Research Grant to Paris and López Bravo.

Supplemental material. The supplementary material for this article can be found at <https://doi.org/10.1017/S09565361250001X>

Supplemental Tables

Supplemental Table S1.1. Summary statistics of 10 sample locations on the Chenalhó square comparative sample.

Supplemental Table S1.2 Component loadings for the first 15 principal components analysis for Jovel Valley samples (major and trace elements).

Supplemental Table S1.3 Importance of components for the first 15 principal components analysis for Jovel Valley samples (major and trace elements).

Supplemental Table S1.4 Component loadings for the first 15 principal components analysis for comparative greenstone samples (major and trace elements).

Supplemental Table S1.5 Importance of components for the first 15 principal components analysis for comparative greenstone samples (major and trace elements).

Supplemental Table S1.6 MANOVA Pillai's trace analysis of trace elements for jadeite comparative samples, by sample provenance groups (Guatemala vs. Chalchihuitán).

Supplemental Table S2.1 Major element concentrations for Jovel Valley greenstone samples.

Supplemental Table S2.2 Trace element concentrations for Jovel Valley greenstone samples.

Supplemental Table S2.3 Major element concentrations for comparative greenstone samples.

Supplemental Table S2.4 Trace element concentrations for comparative greenstone samples.

Supplemental Figures

Supplemental Figure S1.1. Boxplot of elemental concentrations for 10 sample locations on the Chenalhó square comparative sample.

Supplemental Figure S1.2. Biplot of principal components (PC) for elemental concentrations of comparative greenstone specimens, including multiple points of analysis per specimen.

Supplemental Figure S1.3. Biplot of principal components (PC) for elemental concentrations (majors and traces) of comparative greenstone specimens by provenance. The jadeite outlier (J3.3) is characterized by a spot location with an unusually high potassium concentration.

Supplemental Figure S1.4. Biplot of principal components (PC) for elemental concentrations (majors and traces) of comparative greenstone specimens for serpentinite (antigorite/lizardite) specimens. Most samples were sourced from Chenalhó (J4, Chenalhó1, Chenalhó2, Chenalhó3) while J20 was sourced from Huixtán.

Supplemental Figure S1.5. Ternary diagram of trace-element concentrations for ZnK α 1, SbK α 1, and NbK α 1 for jadeite specimens, classified by provenance.

Supplemental Figure S1.6. Principal components analysis (PCA) of all elements (majors and traces) of comparative greenstone specimens, classified by provenance. See Supplemental Tables S1.4 and S1.5.

Supplemental Figure S1.7. Scatterplot matrix of elemental concentrations for Zn, Nb, Sb, and Sr for comparative samples, by provenance group. See Supplemental Table S1.5.

Supplemental Figure S1.8. Principal components analysis (PCA) of trace elements of comparative jadeite specimens, classified by provenance.

Supplemental Figure S1.9. Sample P1. 15 kV, 35 μ A, 180 s, no vacuum, no filter.

Supplemental Figure S1.10. Sample P1. 40 kV, 16.5 μ A, 60 s, no vacuum, Filter 1.

Supplemental Figure S1.11. Sample P2. 15 kV, 35 μ A, 180 s, no vacuum, no filter.

Supplemental Figure S1.12. Sample P2. 15 kV, 35 μ A, 60 s, no vacuum, Filter 1.

Supplemental Figure S1.13. Sample P3. 15 kV, 35 μ A, 180 s, no vacuum, no filter.

Supplemental Figure S1.14. Sample P3. 40 kV, 16.5 μ A, 60 s, no vacuum, Filter 1.

Supplemental Figure S1.15. Sample P4. 15 kV, 35 μ A, 180 s, no vacuum, no filter.

Supplemental Figure S1.16. Sample P4. 40 kV, 16.5 μ A, 60 s, no vacuum, Filter 1.

Supplemental Figure S1.17. Sample P5. 15 kV, 35 μ A, 180 s, no vacuum, no filter.

Supplemental Figure S1.18. Sample P5. 40 kV, 16.5 μ A, 60 s, no vacuum, Filter 1.

Supplemental Figure S1.19. Sample P6. 15 kV, 35 μ A, 180 s, no vacuum, no filter.

Supplemental Figure S1.20. Sample P6. 40 kV, 16.5 μ A, 60 s, no vacuum, Filter 1.

Supplemental Figure S1.21. Sample P7. 15 kV, 35 μ A, 180 s, no vacuum, no filter.

Supplemental Figure S1.22. Sample P7. 40 kV, 16.5 μ A, 60 s, no vacuum, Filter 1.

Supplemental Figure S1.23. Sample P8. 15 kV, 35 μ A, 180 s, no vacuum, no filter.

Supplemental Figure S1.24. Sample P8. 40 kV, 16.5 μ A, 60 s, no vacuum, Filter 1.

Supplemental Figure S1.25. Sample P9. 15 kV, 35 μ A, 180 s, no vacuum, no filter.

Supplemental Figure S1.26. Sample P9. 40 kV, 16.5 μ A, 60 s, no vacuum, Filter 1.

Supplemental Figure S1.27. Sample P10. 15 kV, 35 μ A, 180 s, no vacuum, no filter.

Supplemental Figure S1.28. Sample P10. 40 kV, 16.5 μ A, 60 s, no vacuum, Filter 1.

Supplemental Figure S1.29. Sample P11. 15 kV, 35 μ A, 180 s, no vacuum, no filter. Red = greenstone; green = brown coating

Supplemental Figure S1.30. Sample P11. 40 kV, 16.5 μ A, 60 s, no vacuum, Filter 1. Red = greenstone; green = brown coating

Supplemental Figure S1.31. Sample P12. 15 kV, 35 μ A, 180 s, no vacuum, no filter.

Supplemental Figure S1.32. Sample P12. 40 kV, 16.5 μ A, 60 s, no vacuum, Filter 1.

Supplemental Figure S1.33. Sample P13. 15 kV, 35 μ A, 180 s, no vacuum, no filter.

Supplemental Figure S1.34. Sample P13. 40 kV, 16.5 μ A, 60 s, no vacuum, Filter 1.

Supplemental Figure S1.35. Sample P14a. 15 kV, 35 μ A, 180 s, no vacuum, no filter.

Supplemental Figure S1.36. Sample P14a. 40 kV, 16.5 μ A, 60 s, no vacuum, Filter 1.

Supplemental Figure S1.37. Sample P14b. 15 kV, 35 μ A, 180 s, no vacuum, no filter.

Supplemental Figure S1.38. Sample P14b. 40 kV, 16.5 μ A, 60 s, no vacuum, Filter 1.

Supplemental Figure S1.39. Sample P14c. 15 kV, 35 μ A, 180 s, no vacuum, no filter.

Supplemental Figure S1.40. Sample P14c. 40 kV, 16.5 μ A, 60 s, no vacuum, Filter 1.

Supplemental Figure S1.41. Sample P15. 15 kV, 35 μ A, 180 s, no vacuum, no filter.

Supplemental Figure S1.42. Sample P15. 40 kV, 16.5 μ A, 60 s, no vacuum, Filter 1.

Supplemental Figure S1.43. Sample P17. 15 kV, 35 μ A, 180 s, no vacuum, no filter.

Supplemental Figure S1.44. Sample P17. 40 kV, 16.5 μ A, 60 s, no vacuum, Filter 1.

Supplemental Figure S1.45. Sample P18. 15 kV, 35 μ A, 180 s, no vacuum, no filter.

Supplemental Figure S1.46. Sample P18. 40 kV, 16.5 μ A, 60 s, no vacuum, Filter 1.

Supplemental Figure S1.47. Sample P19. 15 kV, 35 μ A, 180 s, no vacuum, no filter.

Supplemental Figure S1.48. Sample P19. 40 kV, 16.5 μ A, 60 s, no vacuum, Filter 1.

Supplemental Figure S1.49. Sample P20. 15 kV, 35 μ A, 180 s, no vacuum, no filter.

Supplemental Figure S1.50. Sample P20. 40 kV, 16.5 μ A, 60 s, no vacuum, Filter 1.

Supplemental Figure S1.51. Sample J1.1. 15 kV, 35 μ A, 180 s, no vacuum, no filter.

Supplemental Figure S1.52. Sample J1.1. 40 kV, 16.5 μ A, 60 s, no vacuum, Filter 1.

Supplemental Figure S1.53. Sample J1.2. 15 kV, 35 μ A, 180 s, no vacuum, no filter.

Supplemental Figure S1.54. Sample J1.2. 40 kV, 16.5 μ A, 60 s, no vacuum, Filter 1.

Supplemental Figure S1.55. Sample J1.3. 15 kV, 35 μ A, 180 s, no vacuum, no filter.

Supplemental Figure S1.56. Sample J1.3. 40 kV, 16.5 μ A, 60 s, no vacuum, Filter 1.

Supplemental Figure S1.57. Sample J1.4. 15 kV, 35 μ A, 180 s, no vacuum, no filter.

Supplemental Figure S1.58. Sample J1.4. 40 kV, 16.5 μ A, 60 s, no vacuum, Filter 1.

Supplemental Figure S1.59. Sample J1.5. 15 kV, 35 μ A, 180 s, no vacuum, no filter.

Supplemental Figure S1.60. Sample J1.5. 40 kV, 16.5 μ A, 60 s, no vacuum, Filter 1.

Supplemental Figure S1.61. Sample J2.1. 15 kV, 35 μ A, 180 s, no vacuum, no filter.

Supplemental Figure S1.62. Sample J2.1. 40 kV, 16.5 μ A, 60 s, no vacuum, Filter 1.

Supplemental Figure S1.63. Sample J2.2. 15 kV, 35 μ A, 180 s, no vacuum, no filter.

Supplemental Figure S1.64. Sample J2.2. 40 kV, 16.5 μ A, 60 s, no vacuum, Filter 1.

Supplemental Figure S1.65. Sample J2.3. 15 kV, 35 μ A, 180 s, no vacuum, no filter.

Supplemental Figure S1.66. Sample J2.3. 40 kV, 16.5 μ A, 60 s, no vacuum, Filter 1.

Supplemental Figure S1.67. Sample J2.4. 15 kV, 35 μ A, 180 s, no vacuum, no filter.

Supplemental Figure S1.68. Sample J2.4. 40 kV, 16.5 μ A, 60 s, no vacuum, Filter 1.

Supplemental Figure S1.69. Sample J3.1. 15 kV, 35 μ A, 180 s, no vacuum, no filter.

Supplemental Figure S1.70. Sample J3.1. 40 kV, 16.5 μ A, 60 s, no vacuum, Filter 1.

Supplemental Figure S1.71. Sample J3.2. 15 kV, 35 μ A, 180 s, no vacuum, no filter.

Supplemental Figure S1.72. Sample J3.3. 15 kV, 35 μ A, 180 s, no vacuum, no filter.

Supplemental Figure S1.73. Sample J3.3. 40 kV, 16.5 μ A, 60 s, no vacuum, Filter 1.

Supplemental Figure S1.74. Sample J4.1. 15 kV, 35 μ A, 180 s, no vacuum, no filter.

Supplemental Figure S1.75. Sample J4.1. 40 kV, 16.5 μ A, 60 s, no vacuum, Filter 1.

Supplemental Figure S1.76. Sample J4.2. 15 kV, 35 μ A, 180 s, no vacuum, no filter.

Supplemental Figure S1.77. Sample J4.2. 40 kV, 16.5 μ A, 60 s, no vacuum, Filter 1.

Supplemental Figure S1.78. Sample J5.1. 15 kV, 35 μ A, 180 s, no vacuum, no filter.

Supplemental Figure S1.79. Sample J5.1. 40 kV, 16.5 μ A, 60 s, no vacuum, Filter 1.

Supplemental Figure S1.80. Sample J5.2. 15 kV, 35 μ A, 180 s, no vacuum, no filter.

Supplemental Figure S1.81. Sample J5.2. 40 kV, 16.5 μ A, 60 s, no vacuum, Filter 1.

Supplemental Figure S1.82. Sample J6.1. 15 kV, 35 μ A, 180 s, no vacuum, no filter.

Supplemental Figure S1.83. Sample J6.1. 40 kV, 16.5 μ A, 60 s, no vacuum, Filter 1.

Supplemental Figure S1.84. Sample J6.2. 15 kV, 35 μ A, 180 s, no vacuum, no filter.

Supplemental Figure S1.85. Sample J6.2. 40 kV, 16.5 μ A, 60 s, no vacuum, Filter 1.

Supplemental Figure S1.86. Sample J7.1. 15 kV, 35 μ A, 180 s, no vacuum, no filter.

Supplemental Figure S1.87. Sample J7.1. 40 kV, 16.5 μ A, 60 s, no vacuum, Filter 1.

Supplemental Figure S1.88. Sample J7.2. 15 kV, 35 μ A, 180 s, no vacuum, no filter.

Supplemental Figure S1.89. Sample J7.2. 40 kV, 16.5 μ A, 60 s, no vacuum, Filter 1.

Supplemental Figure S1.90. Sample J8.1. 15 kV, 35 μ A, 180 s, no vacuum, no filter.

Supplemental Figure S1.91. Sample J8.1. 40 kV, 16.5 μ A, 60 s, no vacuum, Filter 1.

Supplemental Figure S1.92. Sample J8.2. 15 kV, 35 μ A, 180 s, no vacuum, no filter.

Supplemental Figure S1.93. Sample J8.2. 40 kV, 16.5 μ A, 60 s, no vacuum, Filter 1.

Supplemental Figure S1.94. Sample J9.1. 15 kV, 35 μ A, 180 s, no vacuum, no filter.

Supplemental Figure S1.95. Sample J9.1. 40 kV, 16.5 μ A, 60 s, no vacuum, Filter 1.

Supplemental Figure S1.96. Sample J9.2. 15 kV, 35 μ A, 180 s, no vacuum, no filter.

Supplemental Figure S1.97. Sample J9.2. 40 kV, 16.5 μ A, 60 s, no vacuum, Filter 1.

Supplemental Figure S1.98. Sample J10.1. 15 kV, 35 μ A, 180 s, no vacuum, no filter.

Supplemental Figure S1.99. Sample J10.1. 40 kV, 16.5 μ A, 60 s, no vacuum, Filter 1.

Supplemental Figure S1.100. Sample J10.2. 15 kV, 35 μ A, 180 s, no vacuum, no filter.

Supplemental Figure S1.101. Sample J10.2. 40 kV, 16.5 μ A, 60 s, no vacuum, Filter 1.

Supplemental Figure S1.102. Sample J10.3. 15 kV, 35 μ A, 180 s, no vacuum, no filter.

Supplemental Figure S1.103. Sample J10.3. 40 kV, 16.5 μ A, 60 s, no vacuum, Filter 1.

Supplemental Figure S1.104. Sample J11.1. 15 kV, 35 μ A, 180 s, no vacuum, no filter.

Supplemental Figure S1.105. Sample J11.1. 40 kV, 16.5 μ A, 60 s, no vacuum, Filter 1.

Supplemental Figure S1.106. Sample J11.2. 15 kV, 35 μ A, 180 s, no vacuum, no filter.

Supplemental Figure S1.107. Sample J11.2. 40 kV, 16.5 μ A, 60 s, no vacuum, Filter 1.

Supplemental Figure S1.108. Sample J12.1. 15 kV, 35 μ A, 180 s, no vacuum, no filter.

Supplemental Figure S1.109. Sample J12.1. 40 kV, 16.5 μ A, 60 s, no vacuum, Filter 1.

Supplemental Figure S1.110. Sample J12.2. 15 kV, 35 μ A, 180 s, no vacuum, no filter.

Supplemental Figure S1.111. Sample J12.2. 40 kV, 16.5 μ A, 60 s, no vacuum, Filter 1.

Supplemental Figure S1.112. Sample J13.1. 15 kV, 35 μ A, 180 s, no vacuum, no filter.

Supplemental Figure S1.113. Sample J13.1. 40 kV, 16.5 μ A, 60 s, no vacuum, Filter 1.

Supplemental Figure S1.114. Sample J13.2. 15 kV, 35 μ A, 180 s, no vacuum, no filter.

Supplemental Figure S1.115. Sample J13.2. 40 kV, 16.5 μ A, 60 s, no vacuum, Filter 1.

Supplemental Figure S1.116. Sample J14.1. 15 kV, 35 μ A, 180 s, no vacuum, no filter.

Supplemental Figure S1.117. Sample J14.1. 40 kV, 16.5 μ A, 60 s, no vacuum, Filter 1.

Supplemental Figure S1.118. Sample J14.2. 15 kV, 35 μ A, 180 s, no vacuum, no filter.

Supplemental Figure S1.119. Sample J14.2. 40 kV, 16.5 μ A, 60 s, no vacuum, Filter 1.

Supplemental Figure S1.120. Sample J15.1. 15 kV, 35 μ A, 180 s, no vacuum, no filter.

Supplemental Figure S1.121. Sample J15.1. 40 kV, 16.5 μ A, 60 s, no vacuum, Filter 1.

Supplemental Figure S1.122. Sample J15.2. 15 kV, 35 μ A, 180 s, no vacuum, no filter.

Supplemental Figure S1.123. Sample J15.2. 40 kV, 16.5 μ A, 60 s, no vacuum, Filter 1.

Supplemental Figure S1.124. Sample J20.1.1 15 kV, 35 μ A, 180 s, no vacuum, no filter.

Supplemental Figure S1.125. Sample J20.1.1 40 kV, 16.5 μ A, 60 s, no vacuum, Filter 1.

Supplemental Figure S1.126. Sample J20.2.1 15 kV, 35 μ A, 180 s, no vacuum, no filter.

Supplemental Figure S1.127. Sample J20.2.1 40 kV, 16.5 μ A, 60 s, no vacuum, Filter 1.

Supplemental Figure S1.128. Chenalhó round. 15 kV, 35 μ A, 180 s, no vacuum, no filter.

Supplemental Figure S1.129. Chenalhó round. 40 kV, 16.5 μ A, 60 s, no vacuum, Filter 1.

Supplemental Figure S1.130. Chenalhó square. 15 kV, 35 μ A, 180 s, no vacuum, no filter.

Supplemental Figure S1.131. Chenalhó square. 40 kV, 16.5 μ A, 60 s, no vacuum, Filter 1.

Supplemental Figure S1.132. Chenalhó teardrop. 15 kV, 35 μ A, 180 s, no vacuum, no filter.

Supplemental Figure S1.133. Chenalhó teardrop. 40 kV, 16.5 μ A, 60 s, no vacuum, Filter 1.

Supplemental Figure S1.134. X-ray diffraction pattern of P-1 with phase identification.

Supplemental Figure S1.135. X-ray diffraction pattern of P-2 with phase identification.

Supplemental Figure S1.136. X-ray diffraction pattern of P-3 with phase identification.

Supplemental Figure S1.137. X-ray diffraction pattern of P-4 with phase identification.

Supplemental Figure S1.138. X-ray diffraction pattern of P-5 with phase identification.

Supplemental Figure S1.139. X-ray diffraction pattern of P-6 with phase identification.

Supplemental Figure S1.140. X-ray diffraction pattern of P-7 with phase identification.

Supplemental Figure S1.141. X-ray diffraction pattern of P-8 with phase identification.

Supplemental Figure S1.142. X-ray diffraction pattern of P-9 with phase identification.

Supplemental Figure S1.143. X-ray diffraction pattern of P-10 with phase identification.

Supplemental Figure S1.144. X-ray diffraction pattern of P-11 with phase identification.

Supplemental Figure S1.145. X-ray diffraction pattern of P-12 with phase identification.

Supplemental Figure S1.146. X-ray diffraction pattern of P-13 with phase identification.

Supplemental Figure S1.147. X-ray diffraction pattern of P-14A with phase identification.

Supplemental Figure S1.148. X-ray diffraction pattern of P-14B with phase identification.

Supplemental Figure S1.149. X-ray diffraction pattern of P-14C with phase identification.

Supplemental Figure S1.150. X-ray diffraction pattern of P-15 with phase identification.

Supplemental Figure S1.151. X-ray diffraction pattern of P-17 with phase identification.

Supplemental Figure S1.152. X-ray diffraction pattern of P-18 with phase identification.

Supplemental Figure S1.153. X-ray diffraction pattern of P-19 with phase identification.

Supplemental Figure S1.154. X-ray diffraction pattern of P-20 with phase identification.

Supplemental Figure S1.155. X-ray diffraction pattern of J-1 with phase identification.

Supplemental Figure S1.156. X-ray diffraction pattern of J-2 with phase identification.

Supplemental Figure S1.157. X-ray diffraction pattern of J-3 with phase identification.

Supplemental Figure S1.158. X-ray diffraction pattern of J-4 with phase identification.

Supplemental Figure S1.159. X-ray diffraction pattern of J-5 with phase identification.

Supplemental Figure S1.160. X-ray diffraction pattern of J-6 with phase identification.

Supplemental Figure S1.161. X-ray diffraction pattern of J-7 with phase identification.

Supplemental Figure S1.162. X-ray diffraction pattern of J-8 with phase identification.

Supplemental Figure S1.163. X-ray diffraction pattern of J-9 with phase identification.

Supplemental Figure S1.164. X-ray diffraction pattern of J-10 with phase identification.

Supplemental Figure S1.165. X-ray diffraction pattern of J-11 with phase identification.

Supplemental Figure S1.166. X-ray diffraction pattern of J-12 with phase identification.

Supplemental Figure S1.167. X-ray diffraction pattern of J-13 with phase identification.

Supplemental Figure S1.168. X-ray diffraction pattern of J-14 with phase identification.

Supplemental Figure S1.169. X-ray diffraction pattern of J-15 with phase identification.

Supplemental Figure S1.170. X-ray diffraction pattern of J-17 with phase identification.

Supplemental Figure S1.171. X-ray diffraction pattern of J-20 with phase identification.

Supplemental Figure S1.172. X-ray diffraction pattern of Chenalhó square with phase identification.

Supplemental Figure S1.173. X-ray diffraction pattern of Chenalhó round with phase identification.

Supplemental Figure S1.174. X-ray diffraction pattern of Chenalhó teardrop with phase identification.

References cited

Adams, Richard E. W.

- 1978 Routes of Communication in Mesoamerica: The Northern Guatemalan Highlands and the Peten. In *Mesoamerican Communication Routes and Cultural Contacts*, edited by Thomas A. Lee Jr. and Carlos A. Navarrete, pp. 27–36. Papers of the New World Archaeological Foundation, No. 40. Brigham Young University, Provo, Utah.

Aguilar, María de la Luz

- 2005 Salvamento Arqueológico en la Autopista Tuxtla Gutiérrez-San Cristóbal de Las Casas. *BOLOM* 2:127–146.

Aguilar, Valentina, José Luis Ruvalcaba-Sil, Lauro Bucio, and Eric M. Rivera-Muñoz

- 2019 Characterization and Setting Protocol for a Simultaneous X-Ray Diffraction–X-Ray Fluorescence System (XRD/XRF) for In Situ Analysis. *The European Physical Journal Plus* 134:286. <https://doi.org/10.1140/epjp/i2019-12652-8>.

Aguilar-Melo, Valentina, Alejandro Mitrani, Edgar Casanova-Gonzalez, Mayra D. Manrique-Ortega, Griselda Pérez-Ireta, José Luis Ruvalcaba-Sil, Alejandro Tovalín-Ahumada, Julia Leticia Moscoso-Rincón, Alejandro Sesheña-Hernández, and Josué Lozada-Toledo

2019 Molecular and X-ray Spectroscopies for Noninvasive Characterization of Mayan Green Stones from Bonampak, Chiapas. *Applied Spectroscopy* 73:1074–1086. <https://doi.org/10.1177/0003702819848478>.

Andrieu, Chloé, Edna Rodas, and Luis Luin

- 2014 The Values of Classic Maya Jade: A Reanalysis of Cancuen's Jade Workshop. *Ancient Mesoamerica* 25:141–164. <https://doi.org/10.1017/S0956536114000108>.

Arnauld, M. Charlotte

- 1990 El Comercio Clásico de Obsidiana: Rutas Entre Tierras Altas y Tierras Bajas en el Área Maya. *Latin American Antiquity* 1:347–367.

Bachand, Bruce

- 2013 Las Fases Formativas de Chiapa de Corzo: Nueva Evidencia y Interpretaciones. *Estudios de Cultura Maya* 42:11–52.

Bassie-Sweet, Karen

- 2021 *Maya Gods of War*. University Press of Colorado, Louisville.

Becquelin, Pierre, and Eric Antoine Bosc

- 1973 Notas sobre los Yacimientos de Albita y Jadeíta de San Cristóbal Acasaguastlán, Guatemala. *Estudios de Cultura Maya* 9:67–73.

Berdan, Frances F., and Patricia A. Anawalt

- 1992 *The Codex Mendoza*. University of California Press, Berkeley.

Bernard, Henri Noel, Sara Ladrón de Guevara, Mayra Manrique, and José Luis Ruvalcaba

- 2022 New Approaches to Jadeite Usage in Formative Mesoamerica: Identifying Olmec Portable Sculptures on the Gulf Coast. In *Identities, Experience, and Change in Early Mexican Villages*, edited by Catharina E. Santasillia, Guy David Hepp, and Richard A. Diehl, pp. 108–128. University Press of Florida, Gainesville.

Bishop, Ronald L.

- 2014 Instrumental Approaches to Understanding Mesoamerican Economy: Elusive Promises. *Ancient Mesoamerica* 25:251–269. <https://doi.org/10.1017/S0956536114000157>.

Bishop, Ronald L., Fred W. Lange, and John W. Hoopes

- 1993a Source of Maya and Central American Jadeites: Data Bases and Interpretations. In *Precolumbian Jade: New Geological and Cultural Interpretations*, edited by Fred W. Lange, pp. 125–130. University of Utah Press, Salt Lake City.

Bishop, Ronald L., Edward V. Sayre, J. Mishara, and John W. Hoopes

- 1993b Compositional and Structural Characterization of Mayan and Costa Rican Jadeites. In *Precolumbian Jade: New Geological and Cultural Interpretations*, edited by Fred W. Lange, pp. 30–60. University of Utah Press, Salt Lake City.

Bishop, Ronald L., Edward V. Sayre, and Lambertus van Zelst

- 1985 Characterization of Mesoamerican Jade. In *Applications of Sciences in Examination of Works of Art*, edited by Lambertus van Zelst. Museum of Fine Arts, Boston.

Bosc, Eric Antoine

- 1971 *Geology of the San Agustín Acasaguastlán Quadrangle and Northeastern Part of El Progreso Quadrangle*. Ph.D. dissertation, Rice University, Houston.

Carmack, Robert M.

- 1981 *The Quiché Mayas of Utatlán*. The University of Oklahoma Press, Norman.

Cheung, Kristina A., Nuoya Xie, Zhaoying Yao, Christian Fischer, Vanessa Muros, Sergey Prikhodko, and Ioanna Kakoulli

- 2015 Appendix IV: Materials Analysis. In *Temple of the Night Sun: A Royal Tomb at El Diablo, Guatemala*, edited by Stephen D. Houston,

- Sarah Newman, Edwin Román, and Thomas G. Garrison, pp. 249–257. Precolumbia Mesoweb Press, San Francisco.
- Clark, John E., and Arlene Colman
2014 Olmec Things and Identity: A Reassessment of Offerings and Burials at La Venta, Tabasco. *Archaeological Papers of the American Anthropological Association* 23:14–37. <https://doi.org/10.1111/apaa.12013>.
- Culbert, T. Patrick
1965 *The Ceramic History of the Central Highlands of Chiapas, Mexico*. Papers of the New World Archaeological Foundation, No. 19. Brigham Young University, Provo.
- Curtiss, Brian
1993 Visible and Near-Infrared Spectroscopy for Jade Artifact Analysis. In *Precolumbian Jade: New Geological and Cultural Interpretations*, edited by Fred W. Lange, pp. 73–81. University of Utah Press, Salt Lake City.
- Delgado Robles, Alma A., Jose Luis Ruvalcaba Sil, Pieterjan Claes, Mayra D. Manrique Ortega, Edgar Casanova González, Miguel Ángel Maynez Rojas, Martha Cuevas García, and Sabrina García Castillo
2015 Non-Destructive In Situ Spectroscopic Analysis of Greenstone Objects from Royal Burial Offerings of the Mayan Site of Palenque, Mexico. *Heritage Science* 3:20. <https://doi.org/10.1186/s40494-015-0048-z>.
- Demarest, Arthur A., Chloé Andrieu, Paola Torres, Mélanie Forné, Tomás Barrientos, and Marc Wolf
2014 Economy, Exchange, and Power: New Evidence from the Late Classic Maya Port City of Cancuen. *Ancient Mesoamerica* 25:187–219. <https://doi.org/10.1017/S0956536114000121>.
- Diehl, Richard A.
2005 *The Olmecs: America's First Civilization*. 1st paperback ed. Ancient Peoples and Places, No. 112. Thames & Hudson, London.
- Drucker, Philip, Robert F. Heizer, and Robert J. Squier
1959 Excavations at La Venta, Tabasco, 1955. *Bureau of American Ethnology Bulletin* 170:1–312.
- Englehardt, Joshua D., Mirta A. Insaurralde Caballero, Emiliano R. Melgar Tísoc, Luis R. Velázquez Maldonado, Viridiana Guzmán Torres, Henri Noel Bernard, and Michael D. Carrasco
2020 Digital Imaging and Archaeometric Analysis of the Cascajal Block: Establishing Context and Authenticity for the Earliest Known Olmec Text. *Ancient Mesoamerica* 31: 189–209. <https://doi.org/10.1017/S0956536119000257>.
- Feldman, Lawrence H.
1978 Moving Merchandise in Protohistoric Central Quauhtemallan. In *Mesoamerican Communication Routes and Cultural Contacts*, edited by Thomas A. Lee Jr. and Carlos A. Navarrete, pp. 7–17. Papers of the New World Archaeological Foundation, No. 40. Brigham Young University, Provo.
- Filoy Nadal, Laura (editor)
2010 *Misterios de un rostro maya: La máscara funeraria de K'inich Janaab' Pakal de Palenque*. Instituto Nacional de Anthropología e Historia, Mexico City.
- Fleming, Roberta L.
2007 Micro X-Ray Diffraction (mXRD): A Versatile Technique for Characterization of Earth and Planetary Materials. *Canadian Journal of Earth Sciences* 44:1333–1346. <https://doi.org/10.1139/E07-020>.
- Foshag, William Frederick
1957 *Mineralogical Studies on Guatemalan Jade*. Smithsonian Miscellaneous Collections, Vol. 135, No. 5 (4307). Smithsonian Institution, Washington, DC.
- Franz, Leander, Tay Thye Sun, Henry A. Hänni, Christian De Capitani, Theerapongs Thanasuthipitak, Wilawan Atichat, T. T. Sun, H. A. Hänni, and C. De Capitani
2014 A Comparative Study of Jadeite, Omphacite and Kosmochlor Jades from Myanmar, and Suggestions for a Practical Nomenclature. *The Journal of Gemmology* 34(3):210–229.
- Freidel, David A., Kathryn Reese-Taylor, and David Mora-Marín
2002 The Origins of Maya Civilization: The Old Shell Game, Commodity, Treasure and Kingship. In *Ancient Maya Political Economies*, edited by Marilyn A. Masson and David A. Freidel, pp. 41–86. Altamira Press, Walnut Creek.
- Freidel, David A., and F. Kent Reilly III
2010 The Flesh of the God: Cosmology, Food, and the Origins of Political Power in Ancient Southeastern Mesoamerica. In *Pre-Columbian Footways: Interdisciplinary Approaches to Food, Culture, and Markets in Ancient Mesoamerica*, edited by John E. Staller and Michael Carrasco, pp. 635–680. Springer Science, New York.
- Gallaga Murrieta, Emiliano, and Lowe, Lynne S.
2018 *Chiapa de Corzo: Orígenes de una comunidad milenaria*. Instituto Nacional de Anthropología e Historia, Mexico City.
- Garber, James F., David C. Grove, Kenneth G. Hirth, and John W. Hoopes
1993 Jade Use in Portions of Mexico and Central America. In *Precolumbian Jade: New Geological and Cultural Interpretations*, edited by Fred W. Lange, pp. 211–231. University of Utah Press, Salt Lake City.
- Gendron, François, David C. Smith, and Aicha Gendron-Badou
2002 Discovery of Jadeite-Jade in Guatemala Confirmed by Non-Destructive Raman Microscopy. *Journal of Archaeological Science* 29:837–851.
- González Cruz, Arnoldo
2011 *La reina roja: Una tumba real de Palenque*. CONACULTA; INAH; Turner, Mexico City.
- Hammond, Norman
1972 Obsidian Trade Routes in the Mayan Area. *Science* 178:1092–1093.
1991 *Cuello: An Early Maya Community*. Cambridge University Press, Cambridge.
- Hammond, Norman, Arnold Aspinall, Stuart Feather, John Hazelden, Trevor Gazard, and Stuart Agrell
1977 Maya Jade: Source Location and Analysis. In *Exchange Systems in Prehistory*, edited by Timothy K. Earle and Jonathon E. Ericson, pp. 35–67. Academic Press, New York.
- Harlow, G. E., V. B. Sisson, and S. S. Sorensen
2011 Jadeite from Guatemala: New Observations and Distinctions among Multiple Occurrences. *Geologica Acta* 9:363–387.
- Harlow, George E., Fred W. Lange, and John W. Hoopes
1993 Precolumbian Jade: New Geological and Cultural Interpretations. In *Precolumbian Jade: New Geological and Cultural Interpretations*, edited by Fred W. Lange, pp. 242–250. University of Utah Press, Salt Lake City.
- Hauff, Phoebe L.
1993 The Enigma of Jade, with Mineralogical Reference to Central American Source Materials. In *Precolumbian Jade: New Geological and Cultural Interpretations*, edited by Fred W. Lange, pp. 82–103. University of Utah Press, Salt Lake City.
- He, Bob B., Uwe Preckwinkel, and Kingsley L. Smith
2002 Stress and Texture Analysis with Two-Dimensional X-Ray Diffraction. *Materials Science Forum* 404–407:109–114. <https://doi.org/10.4028/www.scientific.net/MSF.404-407.109>.
- Healy, Paul F., Michael C. Doran, R. Bastian Georg, and Raymond E. March
2018 Mass Spectrometric Analysis of Ancient Maya Greenstone Artifacts from Pacbitun, Belize. *Journal of Archaeological Science: Reports* 19:526–537. <https://doi.org/10.1016/j.jasrep.2018.02.028>.
- Henry, Killian, Jakob Voldum Ahlburg, Henrik L. Andersen, Cecilia Granados Miralles, Marian Stingaciu, Matilde Saura-Múzquiza, and Mogens Christensena
2022 In-Depth Investigations of Size and Occupancies in Cobalt Ferrite Nanoparticles by Joint Rietveld Refinements of X-Ray and Neutron Powder Diffraction Data. *Journal of Applied Crystallography* 55:1336–1350. <https://doi.org/10.1107/S1600576722008123>.
- Hernández-Murillo, Camila, Sergio García-Piedra, Marcela Alfaro-Córdoba, Patricia Fernández-Esquivel, Matthieu Ménager, and Mavis L. Montero
2022 Influence of Surface Roughness on the Spectroscopic Characterization of Jadeite and Greenstones Archaeological Artifacts: The Axe-God Pendants Case Study. *Spectrochimica Acta Part A: Molecular and Biomolecular Spectroscopy* 267:120508. <https://doi.org/10.1016/j.saa.2021.120508>.

- Hernández-Vergara, Rogelio, Elisa Fitz Diaz, Gilles Brocard, and Dante Morán-Zenteno
2021 Illite ⁴⁰Ar–³⁹Ar dating of Eocene Deformation in the Chiapas Fold and Thrust Belt, Southern Mexico. In *The Basins, Orogens and Evolution of the Southern Gulf of Mexico and Northern Caribbean*, edited by I. Davidson, J. N. F. Hull, and J. Pindell, pp. 315–341. Special Publications, No. 50. Geological Society, London.
- Hosler, Dorothy
1994 *The Sounds and Colors of Power: The Sacred Metallurgical Technology of Ancient West Mexico*. MIT Press, Cambridge.
- Houston, Stephen D., Claudia Brittenham, Cassandra Mesick, Alexandre Tokovinine, and Christina Warinner
2009 *Veiled Brightness: A History of Ancient Maya Color*. 1st ed. The William & Bettye Nowlin Series in Art, History, and Culture of the Western Hemisphere. University of Texas Press, Austin.
- Hruby, Zachary X.
2015 Appendix I: Lithics and Minerals. In *Temple of the Night Sun: A Royal Tomb at El Diablo, Guatemala*, edited by Stephen D. Houston, Sarah Newman, Edwin Román, and Thomas G. Garrison, pp. 234–240. Precolumbia Mesoweb Press, San Francisco.
- Hurst, Heather
2009 *Murals and the Ancient Maya Artist: A Study of Art Production in the Guatemalan Lowlands*. Ph.D., Yale University, Connecticut.
- Inomata, Takeshi, Daniela Triadan, Kazuo Aoyama, Victor Castillo, and Hitoshi Yonenobu
2013 Early Ceremonial Constructions at Ceibal, Guatemala, and the Origins of Lowland Maya Civilization. *Science* 340:467–471.
- Inomata, Takeshi, Daniela Triadan, Verónica A. Vázquez López, Juan Carlos Fernández-Díaz, Takayuki Omori, María Belén Méndez Bauer, Melina García Hernández, Timothy Beach, Clarissa Cagnato, and Kazuo Aoyama
2020 Monumental Architecture at Aguada Fénix and the Rise of Maya Civilization. *Nature* 582:530–533. <https://doi.org/10.1038/s41586-020-2343-4>.
- Jaime-Riverón, Olaf
2010 Olmec Greenstone in Early Formative Mesoamerica: Exchange and Process of Production. *Ancient Mesoamerica* 21:123–133. <https://doi.org/10.1017/S095653611000009X>.
- Jaime-Riverón, Olaf, Dolores Tenorio Castilleros, Thomas Calligaro, and Juan Carlos Cruz Ocampo
2009 A Study of Olmec Serpentine: Exchange, Production, Distribution, and Consumption during the Early and Middle Formative Period in Mesoamerica. *Internet Archaeology* 26. <https://doi.org/10.11141/ia.26.21>.
- Juárez-Rodríguez, Octavio, Denisse Argote-Espino, Marco Santos-Ramírez, and Pedro López-García
2018 Portable XRF Analysis for the Identification of Raw Materials of the Red Jaguar Sculpture in Chichén Itzá, Mexico. In “Geoarchaeology: A Toolbox for Revealing Latent Data in Sedimentological and Archaeological Records,” edited by Tara Beuzen-Waller, Friederike Stock, and Yasushisa Kondo. *Quaternary International* 483:148–159. <https://doi.org/10.1016/j.quaint.2017.09.012>.
- Knight, Willow, Faith Gantz, Matthew Carl, Marcus L. Young, Brigitte Kovacevich, Dawn Crawford, Elena Torok, and Fran Baas
2024 Complementary Scientific Techniques for the Study of Mesoamerican Greenstone Objects. *Heritage Science* 12:42. <https://doi.org/10.1186/s40494-023-01128-7>.
- Kovacevich, Brigitte
2006 *Reconstructing Classic Maya Economic Systems: Production and Exchange at Cancuen, Guatemala*. Ph.D., Vanderbilt University, Tennessee.
2013 The Inalienability of Jades in Mesoamerica. *Archaeological Papers of the American Anthropological Association* 23:95–111. <https://doi.org/10.1111/apaa.12018>.
- Kovacevich, Brigitte, and Michael G. Callaghan
2019 Fifty Shades of Green: Interpreting Maya Jade Production, Circulation, Consumption, and Value. *Ancient Mesoamerica* 30:457–472. <https://doi.org/10.1017/S0956536118000184>.
- Kovacevich, Brigitte, Hector Neff, and Ronald L. Bishop
2005 Laser Ablation-ICP-MS Chemical Characterization of Jade from a Jade Workshop at Cancuen, Guatemala. In *Laser Ablation ICP-MS in Archaeological Research*, edited by Robert J. Speakman and Hector Neff, pp. 39–52. University of New Mexico Press, Albuquerque.
- Lesure, Richard G.
1999 On the Genesis of Value in Early Hierarchical Societies. In *Material Symbols: Culture and Economy in Prehistory*, edited by John E. Robb, pp. 23–54. Occasional Papers 26, Center for Archaeological Investigations Southern Illinois University Carbondale, Carbondale.
- Lin, Chenlu, Xuemei He, Zhiyun Lu, and Yuwei Yao
2020 Phase Composition and Genesis of Pyroxenic Jadeite from Guatemala: Insights from Cathodoluminescence. *RSC Advances* 10:15937–15946. <https://doi.org/10.1039/d0ra01772h>.
- Lutterotti, Luca, Federica Dell’Amore, Diego E. Angelucci, Francesco Carrer, and Stefano Gialanella
2016 Combined X-Ray Diffraction and Fluorescence Analysis in the Cultural Heritage Field. *Microchemical Journal* 126:423–430. <https://doi.org/10.1016/j.microc.2015.12.031>.
- Magaloni, Diana, R. Newman, L. Balos, V. Castano, Renato Pancella, and Y. Fruh
1995 An Analysis of Mayan Painting Techniques at Bonampak, Chiapas, Mexico. *MRS Online Proceedings Library* 352:381–388.
- Manrique-Ortega, M. D., E. Casanova-González, A. Mitrani, A. González-Cruz, M. Cuevas-García, and J. L. Ruvalcaba-Sil
2020a Spectroscopic Examination of Red Queen’s Funerary Mask and Her Green Stone Offering from the Mayan Site of Palenque, Mexico. *Spectrochimica Acta Part A: Molecular and Biomolecular Spectroscopy* 234:118205.
- Manrique-Ortega, M. D., Peter Claes, Edgar Casanova-González, José Luis Ruvalcaba-Sil, Ma A. García-Bucio, and Lynne S. Lowe
2014 Non-Invasive Analysis of Green Stone Pieces from Tomb 1 of Chiapa de Corzo, Chiapas. *MRS Online Proceedings Library* 1618:17–29.
- Manrique-Ortega, M. D., A. Mitrani, E. Casanova-González, L. A. Jiménez-Galindo, and J. L. Ruvalcaba-Sil
2019 Methodology for the Non-Destructive Characterization of Jadeite-Jade for Archaeological Studies. *Spectrochimica Acta Part A: Molecular and Biomolecular Spectroscopy* 217:294–309. <https://doi.org/10.1016/j.saa.2019.03.057>.
- Manrique-Ortega, M.D., A. Mitrani, E. Casanova-González, G. Pérez-Ireta, M.A. García-Bucio, I. Rangel-Chávez, V. Aguilar-Melo, O.G. de Lucio, J. L. Ruvalcaba-Sil, N. Sugiyama, and S. Sugiyama
2020b Material Study of Green Stone Artifacts from a Teotihuacan Complex. *Materials and Manufacturing Processes* 35:1431–1445. <https://doi.org/10.1080/10426914.2020.1743855>.
- Masson, Marilyn A., and David A. Freidel
2012 An Argument for Classic Era Maya Market Exchange. *Journal of Anthropological Archaeology* 31:455–484.
- Meanwell, Jennifer, Elizabeth H. Paris, Wilberth Cruz Alvarado, and Carlos Peraza Lope
2013 Metallurgical Ceramics from Mayapán, Yucatán, Mexico. *Journal of Archaeological Science* 40:4306–4318.
- Meanwell, Jennifer L., Elizabeth H. Paris, Carlos Peraza Lope, Linda M. Seymour, and Admir Masic
2020 Blowpipes and Their Metalworking Applications: New Evidence from Mayapán, Yucatán, Mexico. *PLoS One* 15(9):e0238885.
- Melgar, Emiliano, Reyna Solís, and José Luis Ruvalcaba
2012 Technological and Material Characterization of Lapidary Artifacts from Tamtoc Archaeological Site, Mexico. *MRS Online Proceedings Library* 1374:103–114.
- Melgar Tísoc, Emiliano Ricardo, Reyna Beatriz Solís Ciriaco, and Hervé Victor Monterrosa Desruelles
2018 *Piedras de fuego y agua: turquesas y jades entre los nahuas*. Instituto Nacional de Antropología e Historia, Mexico City.
- Mendoza Cuevas, Ariadna, and Luis R. Velázquez Maldonado
2015 Non-Invasive Archaeometrical Study with a Portable Multi-Technique X-Ray System. *Restaurierung und Archäologie* 8:55–61.
- Miller, Mary Ellen, Claudia Brittenham, Heather Hurst, and Leonard Ashby
2013 *The Spectacle of the Late Maya Court: Reflections on the Murals of Bonampak*. 1st ed. The William and Bettye Nowlin Series in Art, History, and Culture of the Western Hemisphere. University of Texas Press, Austin.

- Mora, J. C., M. C. Jaimes-Viera, V. H. Garduño-Monroy, P. W. Layer, V. Pompa-Mera, and M. L. Godínez
2007 Geology and Geochemistry Characteristics of the Chiapanecan Volcanic Arc (Central Area), Chiapas Mexico. *Journal of Volcanology and Geothermal Research* 162:43–72.
- Navarrete, Carlos A.
1978 The Pre-Hispanic System of Communications between Chiapas and Tabasco. In *Mesoamerican Communication Routes and Cultural Contacts*, edited by Thomas A. Lee Jr. and Carlos A. Navarrete, pp. 75–106. Papers of the New World Archaeological Foundation, No. 40. Brigham Young University, Provo.
- Nuttall, Zelia
1901 Chalchihuitl in Ancient Mexico. *American Anthropologist* 3:227–238.
- Ortiz, Ponciano, and María del Carmen Rodríguez
2000 The Sacred Hill of El Manatí: A Preliminary Discussion of the Site's Ritual Paraphernalia. In "Olmec Art and Archaeology in Mesoamerica," edited by John E. Clark and Mary E. Pye. *Studies in the History of Art* 58:74–93.
- Palacios, Enrique Juan
1928 *En los Confines de la Selva Lacandona: Exploraciones en el Estado de Chiapas, Mayo-Agosta 1926*. Contribución de México al XXIII Congreso de Americanistas. Talleres gráficos de la nación, México.
- Paris, Elizabeth H.
2008 Metallurgy, Mayapan and the Postclassic Mesoamerican World System. *Ancient Mesoamerica* 19(1): 43–66. <https://doi.org/10.1017/S0956536108000291>.
2012 *Political Economy in the Postclassic Western Maya Frontier*. Ph.D. dissertation, Department of Anthropology, University of Albany, SUNY. UMI Dissertation Publishing, Proquest LLC, Ann Arbor.
- Paris, Elizabeth H., Elizabeth Baquedano, Carlos Peraza Lope, Marilyn A. Masson, Douglas J. Kennett, Stanley Serafin, and Jennifer L. Meanwell
2022 Metalworking at Mayapán, Yucatan, Mexico: Discoveries from the R-183 Group. *Ancient Mesoamerica* 34:432–454. <https://doi.org/10.1017/S0956536122000128>.
- Paris, Elizabeth H., and Roberto López Bravo
2019 Gulf Coast Influence at Moxviquil, Chiapas, Mexico. *Cambridge Archaeological Journal* 30:183–199. <https://doi.org/10.1017/S0959774319000465>.
2021a Obsidian Exchange Networks in the Jovel Valley, Chiapas, Mexico: A Compositional Analysis Approach. *Journal of Archaeological Science: Reports* 35:102773. <https://doi.org/10.1016/j.jasrep.2020.102773>.
2021b Urban Commerce in the Jovel Valley of Highland Chiapas. *Archaeological Papers of the American Anthropological Association* 32:80–94.
- Paris, Elizabeth H., Roberto López Bravo, and Stanley Serafin
2020 A Funerary Cave at Moxviquil, Chiapas, Mexico. *Journal of Field Archaeology* 45:86–105. <https://doi.org/10.1080/00934690.2019.1693091>.
- Pendergast, David M.
1982 *Excavations at Altun Ha, Belize, 1964–1970*, Vol. 2. Royal Ontario Museum, Toronto.
1998 Dressed to Kill: Jade Beads and Pendants in the Maya Lowlands. *BEADS: Journal of the Society of Bead Researchers* 10:3–12.
- Powis, Terry G., Sherman Horn III, Gyles Iannone, Paul F. Healy, James F. Garber, Jaime J. Awe, Sheldon Skaggs, and Linda A. Howie
2016 Middle Preclassic Period Maya Greenstone "Triangulates": Forms, Contexts, and Geology of a Unique Mesoamerican Groundstone Artifact Type. *Journal of Archaeological Science: Reports* 10:59–73.
- Rochette, Erick T.
2009 *The Late Classic Organization of Jade Artifact Production in the Middle Motagua Valley, Zacapa, Guatemala*. Ph.D. dissertation, Department of Anthropology, Pennsylvania State University.
- Ruvalcaba, José Luis, Emiliano Melgar, and Thomas Calligaro
2011 Manufacturing Analysis and Non-Destructive Characterisation of Green Stone Objects from the Tenochtitlan Templo Mayor Museum, Mexico. In *Proceedings of the 37th International Symposium on Archaeometry, 13th–16th May 2008, Siena, Italy*, edited by Isabella Turbanti-Memmi, pp. 299–304. Springer Berlin Heidelberg, Berlin, Heidelberg. https://doi.org/10.1007/978-3-642-14678-7_43.
- Ruvalcaba, José Luis, Linda Manzanilla, Emiliano Melgar, and R. Lozano Santa Cruz
2008 PIXE and Ionoluminescence for Mesoamerican Jadeite Characterization. *X-Ray Spectrometry* 37:96–99. <https://doi.org/10.1002/xrs.1026>.
- Sahagún, Bernardino de
1959 *General History of the Things of New Spain; Florentine Codex, Book 9–The Merchants*. Translated by Arthur J. O. Anderson and Charles E. Dibble. School of American Research, Santa Fe.
1963 *General History of the Things of New Spain; Florentine Codex, Book 11–Earthly Things*. Translated by Arthur J. O. Anderson and Charles E. Dibble. 14 vols. School of American Research, Santa Fe.
- Seitz, Russell, George E. Harlow, Virginia B. Sisson, and Karl E. Taube
2001 "Olmec Blue" and Formative Jade Sources: New Discoveries in Guatemala. *Antiquity* 75:687–688.
- Simmons, Scott E., David M. Pendergast, and Elizabeth Graham
2009 The Context and Significance of Copper Artifacts in Postclassic and Early Historic Lamanai, Belize. *Journal of Field Archaeology* 34:57–75.
- Simmons, Scott E., and Aaron N. Shugar
2013a Archaeometallurgy at Lamanai, Belize: New Discoveries and Insights from the Southern Maya Lowland Area. In *Archaeometallurgy in Mesoamerica: Current Approaches and New Perspectives*, edited by Scott E. Simmons and Aaron N. Shugar, pp. 135–159. University Press of Colorado, Boulder.
2013b Maya Metallurgical Technology in Late Postclassic-Spanish Colonial Times: The View from Lamanai, Belize. *Archaeosciences* 37:105–121.
- Smith, A. L., and A. V. Kidder
1943 Explorations in the Motagua Valley, Guatemala. In *Contributions to American Archaeology and History*, pp. 101–182. Publication 546, Carnegie Institution of Washington, Washington, DC.
- Smith, David C., and François Gendron
1997 Archaeometric Application of the Raman Microprobe to the Non-Destructive Identification of Two Pre-Columbian Ceremonial Polished "Greenstone" Axe-Heads from Mesoamerica. *Journal of Raman Spectroscopy* 28:731–738. [https://doi.org/10.1002/\(SICI\)1097-4555\(199709\)28:9](https://doi.org/10.1002/(SICI)1097-4555(199709)28:9).
- Smith, David C.
2005 Case Study: Mesoamerican Jade. In *Raman Spectroscopy in Archaeology and Art History*, edited by Howell G. M. Edwards and John M. Chalmers, pp. 412–427. Royal Society of Chemistry, London.
- Smith, J. Lawrence
1851 Memoir on Emery - Second Part - On the Minerals Associated with Emery: Corundum, Hydrargillite, Diaspore, Zinc Spinel, Pholerite, Ephesite (A New Species), Emerylite (A New Species), Muscovite, Chloritoid (A New Variety), Black Tourmaline, Chlorite, Magnetic Oxid of Iron, Oligiste Iron, Hydrated Oxid of Iron, Iron Pyrites, Rutile, Ilmenite and Titaniferous Iron. *American Journal of Science and Arts, Second Series*, 11-12:53–66.
- Smith, Michael E.
1996 The Strategic Provinces. In *Aztec Imperial Strategies*, edited by Frances F. Berdan, Richard E. Blanton, Elizabeth Hill Boone, Mary G. Hodge, Michael E. Smith, and Emily Umberger, pp. 137–150. Dumbarton Oaks Research Library and Collection, Washington, DC.
- Solórzano, Sofia, Miguel Angel Castillo-Santiago, Dario Alejandro Navarrete-Gutierrez, and Ken Oyama
2003 Impacts of the Loss of Neotropical Highland Forests on the Species Distribution: A Case Study Using Resplendent Quetzal an Endangered bird Species. *Biological Conservation* 114:341–349.
- Taladoire, Eric
2016 Las bases económicas de una entidad política maya. El caso de Toniná. *Estudios de cultura maya* 48:11–37.
- Taube, Karl A., and Reiko Ishihara-Brito
2012 From Stone to Jewel. In *Ancient Maya Art at Dumbarton Oaks*, edited by Joanne Pillsbury, Miriam Doutriaux, Reiko Ishihara-Brito, and Alexandre Tokovinine, pp. 134–153. Dumbarton Oaks, Washington, DC.
- Taube, Karl A., Virginia B. Sisson, Russell Seitz, and George E. Harlow
2004 The Sourcing of Mesoamerican Jade: Expanded Geological Reconnaissance in the Motagua Region, Guatemala. In *Olmec Art and Dumbarton Oaks*, edited by Karl A. Taube. Pre-Columbian Art at Dumbarton Oaks, No. 2, pp. 203–228. Dumbarton Oaks, Washington, DC.

- Tozzer, Alfred M.
1941 *Landa's Relacion De Las Cosas De Yucatan: A Translation*. Peabody Museum Papers, Vol. 18, No. 1. Peabody Museum Press, Cambridge.
- Tremain, Cara Grace
2014 Pre-Columbian "Jade": Towards an Improved Identification of Green-Colored Stone in Mesoamerica. *Lithic Technology* 39:137–150. <https://doi.org/10.1179/0197726114Z.00000000044>.
- Urban, Patricia A., Aaron N. Shugar, Laura Richardson, and Edward Schortman
2013 The Production of Copper at El Coyote, Honduras: Processing, Dating, and Political Economy. In *Archaeometallurgy in Mesoamerica: Current Approaches and New Perspectives*, edited by Scott E. Simmons and Aaron N. Shugar, pp. 77–112. University of Colorado Press, Boulder.
- Viqueira, Juan Pedro
2006 Ires y Venires de los Caminos de Chiapas (Épocas Prehispanica y Colonial). In *Rutas de la Nueva Espana*, edited by Chantal Cramaussel, pp. 137–176. El Colegio de Michoacán.
- Viqueira Albán, Juan Pedro
1999 *El lento, aunque inexorable desmembramiento del señorío de Zinacantán*. Centro de Estudios Superiores de México y Centroamérica Anuario 98, pp. 312–342. Universidad de Ciencias y Artes de Chiapas.
- Wasserstrom, Robert
1983 *Class and Society in Central Chiapas*. University of California Press, Berkeley.
- Weeks, John M.
2013 Late Prehistoric K'iche' Metalworking at Uxatán, Guatemala. In *Archaeometallurgy in Mesoamerica: Current Approaches and New Perspectives*, edited by Scott E. Simmons and Aaron N. Shugar, pp. 113–133. University Press of Colorado, Boulder.
- Woodfill, Brent K.S., and Chloé Andrieu
2012 Tikal's Early Classic Domination of the Great Western Trade Route: Ceramic, Lithic, and Iconographic Evidence. *Ancient Mesoamerica* 23:189–209. <https://doi.org/10.1017/S0956536112000156>.